Fatty Acid Analogue N-Arachidonoyl Taurine Restores Function of I_{Ks} Channels with Diverse Long QT Mutations

Sara I Liin[1,2*], Johan E Larsson[2], Rene Barro-Soria[1], Bo Hjorth Bentzen[3] and H Peter Larsson[1*]

[1] Department of Physiology and Biophysics, University of Miami, Miami, FL 33136, USA

[2]Department of Clinical and Experimental Medicine, Linköping University, SE-581 85 Linköping, Sweden

[3]The Danish Arrhythmia Research Centre and Department of Biomedical Sciences, University of Copenhagen, DK-2200 Copenhagen, Denmark

*Corresponding authors:

H.P.L., Department of Physiology and Biophysics, University of Miami, Miami, FL 33136, USA. +1 305 243 1021. PLarsson@med.miami.edu

or

S.I.L., Department of Clinical and Experimental Medicine, Linköping University, SE-581 85 Linköping, Sweden. +46 10 103 4371. sara.liin@liu.se

Abstract

About 300 loss-of-function mutations in the I_{Ks} channel have been identified in patients with Long QT syndrome and cardiac arrhythmia. How specific mutations cause arrhythmia is largely unknown and there are no approved I_{Ks} channel activators for treatment of these arrhythmias. We find that several Long QT syndrome-associated I_{Ks} channel mutations shift channel voltage dependence and accelerate channel closing. Voltage-clamp fluorometry experiments and kinetic modeling suggest that similar mutation-induced alterations in I_{Ks} channel currents may be caused by different molecular mechanisms. Finally, we find that the fatty acid analogue N-arachidonoyl taurine restores channel gating of many different mutant channels, even though the mutations are in different domains of the I_{Ks} channel and affect the channel by different molecular mechanisms. N-arachidonoyl taurine is therefore an interesting prototype compound that may inspire development of future I_{Ks} channel activators to treat Long QT syndrome caused by diverse I_{Ks} channel mutations.

Introduction

Long QT syndrome (LQTS) is a condition of the heart which in most cases is caused by a mutation in cardiac ion channels[1, 2]. In LQTS, the action potential of the heart is prolonged, which is observed as a prolonged QT interval in the electrocardiogram. LQTS patients have an increased risk of developing ventricular tachyarrhythmias called *torsades de pointes* when exposed to triggers such as adrenergic stress[2, 3]. These arrhythmias can cause palpitation, syncope or sudden death due to ventricular fibrillation. To improve the clinical outcome of LQTS patients, it is therefore critical to prevent these LQTS-induced life-threatening arrhythmias.

Most mutations causing LQTS are located in the *KCNQ1* gene[1]. *KCNQ1* codes for the potassium channel $K_V7.1$, which in the heart co-assembles with the beta-subunit KCNE1 to form the slowly-activating, voltage-dependent potassium channel I_{Ks}[4, 5]. The I_{Ks} channel provides one of the important delayed rectifier outward potassium currents that repolarizes the cardiomyocyte and terminates the cardiac action potential[6]. Reduced I_{Ks} function therefore tends to delay cardiomyocyte repolarization, thereby causing prolonged cardiac action potential durations and a prolonged QT interval. The cardiac I_{Ks} channel consists of four $K_V7.1$ subunits and two to four KCNE1 subunits[7-9]. Throughout this work, we will refer to the I_{Ks} channel as $K_V7.1$+KCNE1. $K_V7.1$ has six transmembrane segments named S1-S6[10] (**Fig. 1a**). S1-S4 of each $K_V7.1$ subunit forms a voltage-sensing domain where S4 is the voltage sensor with three positive gating charges. S5 and S6 from all four $K_V7.1$ subunits form the pore domain with a putative gate in S6 that needs to move to open the ion-conducting pore of the channel. KCNE1 has a single-transmembrane segment (**Fig. 1a**) and is proposed to be localized in the otherwise lipid-filled space between two voltage-sensing domains of neighbouring $K_V7.1$ subunits[11]. Upon cardiomyocyte depolarization, the voltage

sensor of K_V7.1 moves outward in relation to the membrane. It has been proposed that this movement of the voltage sensor is transferred to the pore domain via the S4-S5 linker and induces channel opening by moving the S6 gate[10].

Altogether, about 300 mutations in *KCNQ1* and *KCNE1* have been identified in patients suffering from LQTS[1] (http://www.fsm.it/cardmoc/). These mutations are distributed throughout the channel sequence and are therefore likely to cause channel dysfunction by different mechanisms, which are, however, largely unknown. Potential mechanisms for K_V7.1+KCNE1 channel loss of function by a mutation could, for example, be interference with voltage sensor movement, gate opening, or membrane expression. LQTS is today treated with drugs that prevent the triggering of arrhythmic activity, such as beta-blockers, or with arrhythmia-terminating implantable cardioverter defibrillator[1]. A different treatment strategy for LQTS caused by loss-of-function mutations in the K_V7.1+KCNE1 channel would be to pharmacologically augment the K_V7.1+KCNE1 channel function of these LQTS mutants, thereby shortening the prolonged QT interval and lower the risk of arrhythmia development. However, there is currently no clinically approved K_V7.1+KCNE1 channel activator.

In this study, we investigate the biophysical properties and potential mechanism of action of LQTS-associated K_V7.1+KCNE1 channel mutations and test the ability of the fatty acid analogue N-arachidonoyl taurine (N-AT) to restore the function of these mutants.
We selected eight mutations of residues mutated in patients with LQTS located in different segments of the K_V7.1+KCNE1 channel and that were previously shown to form active channels[12-19]. We measure the movement of the S4 voltage sensor in selected mutants using voltage clamp fluorometry to further our understanding of the molecular mechanisms underlying the defects caused by the diverse mutations. We find that the eight LQTS-

87 associated mutants affect the voltage dependence and/or closing kinetics, in some cases by
88 different molecular mechanisms. Moreover, we find that N-AT restores much of the channel
89 activity in these eight LQTS-associated K_V7.1+KCNE1 mutants. This suggests that N-AT
90 may function as a general activator of K_V7.1+KCNE1 channels with diverse mutational
91 defects.
92

93 ## *Results*

94 ### *LQTS mutants show altered biophysical properties*

95 We first study the biophysical properties of six point mutations in K_V7.1 (F193L, V215M,
96 S225L, L251P, F351S, R583C), and two in KCNE1 (K70N, S74L) identified in patients with
97 LQTS[13, 17, 19-22] (**Fig. 1a**). As L251P and F351S did not produce functional channels[21, 23] (**Fig.**
98 **1 – figure supplement 1**), we engineered the milder L251A and F351A mutants instead.
99 L251A and F351A will be referred to as "LQTS-like mutants". When expressed alone in
100 *Xenopus* oocytes, all investigated K_V7.1 mutants, except F193L and V215M, display a shifted
101 conductance *versus* voltage curve ($G(V)$) compared to the wild-type K_V7.1 channel (**Fig. 1 –**
102 **figure supplement 2**; **Supplementary File 1**). S225L, L251A and F351A shift the $G(V)$
103 towards positive voltages compared to wild-type K_V7.1. In contrast, R583C shifts the half-
104 maximal activation, V_{50}, ~10 mV towards negative voltages compared to wild-type K_V7.1.
105 This apparent negative shift is likely caused by the pronounced inactivation of the R583C
106 mutant (**Fig. 1 – figure supplement 3a**), which is seen to considerable smaller extent in the
107 other K_V7.1 mutants and wild-type K_V7.1 (inset in **Fig. 1 – figure supplement 3a**). When a
108 fraction of channels are released from inactivation, by introducing a brief hyperpolarizing
109 pulse between the test pulse and the tail pulse, R583C has a V_{50} fairly comparable to wild-
110 type K_V7.1 (**Fig. 1 – figure supplement 3b**).

When the $K_V7.1$ mutants are co-expressed with KCNE1, all $K_V7.1$ and KCNE1 mutants except $K_V7.1$/F193L+KCNE1 have a $G(V)$ that is shifted towards positive voltages compared to the wild-type $K_V7.1$+KCNE1 channel (**Fig. 1b**). $K_V7.1$/F351A causes the most dramatic change by shifting V_{50} more than +30 mV. We are therefore only able to record the foot of the $G(V)$ curve of $K_V7.1$/F351A+KCNE1, and a shift in V_{50} of +30 mV is a lower estimate of the change in V_{50} (ΔV_{50}). One of the other mutants with dramatically shifted $G(V)$ is $K_V7.1$/S225L+KCNE1. V_{50} for $K_V7.1$/S225L+KCNE1 is shifted almost +30 mV compared to wild-type $K_V7.1$+KCNE1 (**Fig. 1c**; **Supplementary File 1**). S225L also slows down $K_V7.1$+KCNE1 channel opening kinetics ($P < 0.01$; **Fig. 1d**; **Supplementary File 1**). All mutants, except for L251A, accelerate channel closing kinetics compared to wild-type $K_V7.1$+KCNE1 (**Supplementary File 1**). K70N has the most dramatic effect on $K_V7.1$+KCNE1 channel closing by accelerating the closing kinetics by approximately a factor of 5 (**Fig. 1e**; **Supplementary File 1**). When comparing the amplitude of K^+ currents generated by these mutants with the current amplitude of the wild-type $K_V7.1$+KCNE1 channel in the same batch of oocytes, we note that all mutants generate smaller currents than wild-type over a large voltage range (**Fig. 1 – figure supplement 4**). Although defective trafficking may contribute to these reduced currents in *Xenopus* oocytes, the current amplitudes for most mutants matches fairly well with the predicted current amplitude from channels with $G(V)$ curves shifted towards positive voltages as observed for these mutants (**Fig. 1 – figure supplement 4a**), suggesting that the reduced current amplitudes in *Xenopus* oocytes are mainly a result of gating defects (and not trafficking defects).

To summarize, all mutations change channel function by altering voltage dependence of opening and/or the kinetics of opening and/or closing. Reduced function of the

K_V7.1+KCNE1 channel induced by these LQTS and LQTS-like mutations may largely be explained by the right-shifted $G(V)$ and the faster closing kinetics caused by these mutations. F193L does not alter the $G(V)$, but speeds up K_V7.1+KCNE1 channel closing by a factor of 2 (**Supplementary File 1**). These results are consistent with previous reported findings for some of these mutants[12-18].

Heterozygous expression reduces LQTS mutant severity

Patients with LQTS mutations can be either homozygous or heterozygous for the mutation. To mimic heterozygous expression, we co-inject the mutated K_V7.1 subunit and KCNE1 subunit together with the wild-type K_V7.1 subunit (or wild-type KCNE1 subunit for KCNE1 mutants) (cartoon in **Fig. 2**). We refer to this as heterozygous expression. Figure 2a-b compares homozygous expression ($K_V7.1^{wt}$+$KCNE1^{mut}$ or $K_V7.1^{mut}$+$KCNE1^{wt}$) with heterozygous expression ($K_V7.1^{wt}$+$K_V7.1^{mut}$+$KCNE1^{wt}$ or $K_V7.1^{wt}$+$KCNE1^{wt}$+$KCNE1^{mut}$) for K_V7.1/S225L (**Fig. 2a**) and KCNE1/K70N (**Fig. 2b**). Both of these examples show that heterozygous expression generates channels with more wild-type like opening or closing kinetics and $G(V)$ compared to homozygous expression of the mutant subunit. A milder biophysical phenotype upon heterozygous expression is generally seen for the LQTS and LQTS-like mutants in terms of $G(V)$, current amplitude, and/or closing kinetics (**Fig. 2c-d**, **Fig. 1 – figure supplement 4**, **Supplementary File 2**). This milder phenotype indicates that the wild-type subunit can partly restore K_V7.1+KCNE1 function. Alternatively, for mutants with a $G(V)$ that is very shifted to positive voltages (e.g. F351A), it may be that channel complexes that contain the mutated subunits are largely out of the physiological voltage range and therefore do not contribute substantially to the recorded current. Also, for mutants with low membrane expression (e.g. possibly F193L[13]), it may be that channels containing

160 the wild-type subunit are favoured so that in most K_V7.1+KCNE1 channel complexes the
161 majority (or all) of the subunits will be wild-type subunits.
162

163 ***Different mutants display different fluorescence versus voltage profiles***

164 Although most of the mutants shift channel voltage dependence and affect channel closing
165 kinetics, the underlying mechanism of mutation-induced changes in K_V7.1+KCNE1 channel
166 function is most likely different for different mutations. For instance, mutations located in S5
167 and S6 (e.g. F351A) may mainly affect gate movement, while mutations in S1-S4 (e.g.
168 S225L) are more likely to affect voltage sensor movement. To explore whether different
169 mutations interfere with different gating transitions, we use voltage clamp fluorometry, in
170 which the movement of the voltage sensor in K_V7.1 can be tracked by the fluorescence
171 change from the fluorescent probe Alexa-488-maleimide attached to G219C in the S3-S4
172 loop (referred to as G219C*)[24-26]. Voltage sensor movement (measured by fluorescence) and
173 gate movement (measured by ionic currents) are then monitored under two-electrode voltage
174 clamp. The K_V7.1/G219C* construct by itself or co-expressed with KCNE1 gives voltage-
175 dependent fluorescence changes (**Fig. 3a**). As previously reported, the fluorescence *versus*
176 voltage ($F(V)$) curve of K_V7.1/G219C* correlates well with the $G(V)$ curve (**Fig. 3a**, left
177 panel), while the $F(V)$ curve of K_V7.1/G219C*+KCNE1 is divided into two components (**Fig.**
178 **3a**, right panel)[24-26]. For K_V7.1/G219C*+KCNE1, the first fluorescence component ($F1$) has
179 been suggested to represent the main voltage sensor movement and the second fluorescence
180 component ($F2$) to be correlated with gate opening[24]. We introduce G219C into K_V7.1/S225L
181 and K_V7.1/F351A. The $G(V)$ curves of both K_V7.1/G219C*/S225L and
182 K_V7.1/G219C*/F351A are shifted towards more positive voltages compared to the wild-type
183 channel, but the $F(V)$ curves are differentially affected by the two mutations (**Fig. 3b-c**, left
184 panels). For K_V7.1/G219C*/S225L, the $F(V)$ curve is shifted to a similar extent as the $G(V)$

curve, while for K_V7.1/G219C*/F351A, the $F(V)$ curve is shifted to a considerably smaller extent[25]. When these mutants are co-expressed with KCNE1, we observe different effects on the voltage dependence of the two fluorescent components $F1$ and $F2$ induced by the mutations. The S225L mutation primarily shifts $F1$ towards positive voltages so that $F1$ and $F2$ of K_V7.1/G219C*/S225L+KCNE1 are hardly distinguishable in the $F(V)$ curve (**Fig. 3b**, right panel). In contrast, the F351A mutation primarily shifts $F2$ towards positive voltages so that $F1$ and $F2$ are clearly separated (**Fig. 3c**, right panel). Thus, S225L and F351A seem to shift the $G(V)$ curve of K_V7.1+KCNE1 towards positive voltages by interfering with different gating transitions.

Kinetic modeling recapitulates experimental findings

To further explore the different effects of S225L and F351A in the voltage-clamp fluorometry experiments, we use two kinetic models previously developed to reproduce the currents and fluorescence from K_V7.1/G219C*[26] and K_V7.1/G219C*+KCNE1 channels[24], respectively. The K_V7.1/G219C* model is an allosteric model with 10 states (**Fig. 3 – figure supplement 1a**), where the horizontal transition is the main S4 movement (which generates the main fluorescence component $F1$) and the vertical transition is channel opening accompanied by an additional smaller S4 movement (that generates a smaller additional fluorescence component $F2$)[26, 27]. The K_V7.1/G219C* model allows for channel opening after only a subset of four S4s are activated, which thereby generates $F(V)$ and $G(V)$ that are close in voltage dependence (reference[26]; and **Fig. 3 –figure supplement 2a**). The K_V7.1/G219C*+KCNE1 model has 6 states (**Fig. 3 – figure supplement 1b**), where the horizontal transition is the main S4 movement (which generates the main fluorescence component $F1$) and the vertical transition is channel opening accompanied by an additional smaller S4 movement (that generates a smaller additional fluorescence component $F2$)[26, 27]. The K_V7.1/G219C*+KCNE1 model only allows for channel opening after all four S4s are

activated, which thereby generates $F(V)$ and $G(V)$ that are separated in voltage dependence (reference[24]; and **Fig. 3 –figure supplement 2a**).

Using these models, we can reproduce the main features of the fluorescence and currents from K_V7.1/G219C*/S225L and K_V7.1/G219C*/S225L+KCNE1 by only shifting the main voltage sensor movement by +50 mV in both models (**Fig. 3 –figure supplement 2b**), as if the S225L mutation mainly affects the main S4 movement. In the K_V7.1 model, shifting the main voltage sensor movement by +50 mV shifts both the $G(V)$ and $F(V)$ curves by +35-40 mV, similar to the effect induced by the S225L mutation in the experimental data. In the K_V7.1+KCNE1 model, shifting the main voltage sensor movement by +50 mV results in that the $F1$ and $F2$ components overlap in voltage, such that it is hard to distinguish the two components, and that the $G(V)$ is shifted by +10 mV. Both effects are similar to the effects induced by the S225L mutation in the experimental data (cf. Fig. 3b).

We can reproduce the main features of the fluorescence and currents from K_V7.1/G219C*/F351A and K_V7.1/G219C*/F351A+KCNE1 by only shifting the voltage dependence of the opening transition by +140 mV in both models (**Fig. 3 –figure supplement 2c**), as if the F351A mutation mainly affects the opening transition. In the K_V7.1 model, shifting the opening transition by +140 mV shifts the $G(V)$ by +100 mV whereas the $F(V)$ is shifted less and has a shallower slope, similar to the effects induced by the F351A mutation in the experimental data. In the K_V7.1+KCNE1 model, shifting the opening transition by +140 mV results in that the $F1$ and $F2$ components are further separated in voltage and that the $G(V)$ is shifted by +100 mV. Both effects are similar to the effects induced by the F351A mutation in the experimental data (cf. Fig. 3c).

In summary, our voltage-clamp fluorometry experiments together with kinetic modeling are compatible with a model in which the S225L mutant primarily interferes with the main S4 movement, whereas the F351A mutant interferes with later gating transitions associated with pore opening. One note of caution is that the interpretation of the mutational effects is dependent on the models used for the wild-type channels. Other models for $K_V7.1$ and $K_V7.1$+KCNE1 channels have been proposed[27, 28], but these have not been as extensively tested or developed as our models. Although other alternative mechanisms for the effects of these mutations are possible, the different impacts of S225L and F351A on the fluorescence *versus* voltage relationships suggest that these mutations introduce distinct molecular defects.

N-AT enhances the activity of all tested LQTS and LQTS-like mutants

We previously observed that the effect of regular polyunsaturated fatty acids, such as docosahexaenoic acid, on $K_V7.1$ is impaired by co-expression with the KCNE1 subunit[29]. In contrast, we found that the PUFA analogue N-arachidonoyl taurine (N-AT, structure in **Fig. 4**) retained its ability to activate the $K_V7.1$ channel also in the presence of KCNE1. N-AT activated the wild-type $K_V7.1$+KCNE1 by shifting the $G(V)$ roughly –30 mV[29] (**Fig. 4 – figure supplement 1**). The magnitude of this N-AT-induced shift is comparable to, but in opposite direction, to the $G(V)$ shifts observed for several of the LQTS and LQTS-like mutants. We therefore here test the ability of N-AT to enhance the function of the eight $K_V7.1$+KCNE1 mutant channels. Figure 4a-b shows representative effects of 7-70 μM N-AT on $K_V7.1$/S225L+KCNE1. 70 μM N-AT increases current amplitude by a factor of 16 at +20 mV (**Fig. 4a**) and shifts the $G(V)$ curve by about –50 mV (**Fig. 4b**, **Supplementary File 3**). Steady state of N-AT effects is reached within a few minutes (**Fig. 4 – figure supplement 2**). We note a small instantaneous 'leak' component in the 70 μM N-AT trace of $K_V7.1$/S225L+KCNE1 (**Fig. 4a**). This leak component in $K_V7.1$/S225L+KCNE1 is observed

also in the absence of N-AT, but at more positive voltages (**Fig. 4 – figure supplement 3**). We do not observe this leak component in wild-type K_V7.1+KCNE1 upon application of N-AT (**Fig. 4 – figure supplement 1a**), which suggests that this phenomenon is associated with the S225L mutation. The human ventricular action potential has duration of about 300-400 ms and a systolic voltage range of about 0 to +40 mV[30, 31]. To test the behaviour of the S225L mutation during shorter stimulating pulses, we apply repetitive 300-ms pulses to +40 mV at a frequency of 1 Hz and at 28°C (37°C was not tolerated by the oocytes). In response to this protocol, the K_V7.1/S225L+KCNE1 channel barely opens and thus generates only minor currents (**Fig. 4c**). In contrast, we observe large K_V7.1/S225L+KCNE1 currents upon application of 70 µM N-AT (**Fig. 4c**). N-AT also restores the gradual increase in current amplitude during repetitive pulsing seen experimentally (inset in **Fig. 4c**) and in computer simulations[32] for the wild-type K_V7.1+KCNE1 channel.

Further testing of N-AT show that 70 µM N-AT shifts the $G(V)$ curve of all tested mutants by 30-50 mV towards more negative voltages (**Fig. 4d-e**, **Supplementary File 3**). The $G(V)$ curve of wild-type K_V7.1+KCNE1 is shifted by –27.0 ± 2.5 mV[29]. Thus, 70 µM N-AT completely corrects the positive $G(V)$ shifts induced by the mutations so that in the presence of N-AT the $G(V)$ is similar to or shifted negative compared to the $G(V)$ of the wild-type K_V7.1+KCNE1 channel (**Fig. 4d**, F351A homozygous expression was not included in this analysis because of the very shifted $G(V)$ curve of this mutant). The $G(V)$ of mutants is shifted about equally by N-AT for homozygous and heterozygous expression (**Fig. 4e**). The slope of the $G(V)$ curve varies slightly (10.4 to 16.3) among the mutants (**Supplementary File 3**). To correct for this difference in slope and to better compare the functional effect of N-AT-induced $G(V)$ shifts on the different mutants, we also calculate the change in Gibbs free energy for channel opening ($\Delta\Delta G_o$) that 70 µM N-AT induces. 70 µM N-AT reduces the

energy required to open the channel by 5.3-9.0 kJ/mol depending on mutant (4.9 ± 0.7 kJ/mol (n = 5) for wild-type) (**Fig. 4f**). To estimate the functional effect of N-AT on the K_V7.1+KCNE1 current amplitude of each mutant, we calculate the ratio of the current amplitude at the end of the 5-s test pulse before and after application of N-AT at +20 and +40 mV. The 5-s voltage pulse to +20 mV (or +40 mV) at room temperature was chosen to make the K_V7.1+KCNE1 channel activate to a similar extent as during a ventricular action potential (300-400 ms) at body temperature (note that K_V7.1+KCNE1 channels have a relatively high Q_{10} of around 5-7.5[33, 34]). 70 μM N-AT increases the current amplitude of all mutants at these voltages (**Fig. 4 – figure supplement 4a-b**, **Supplementary File 3**). As expected, current amplitude is most increased for those mutants that have the most shifted $G(V)$ curve towards more positive voltages (e.g. V215M and S225L). This is because these mutants are still at the foot of their $G(V)$ curve at +20 and +40 mV and a N-AT-induced shift towards more negative voltages results in a relatively larger increase in the current amplitude. By multiplying these relative N-AT-induced increases in current amplitude with the relative current amplitude of each mutant (compared to wild-type K_V7.1+KCNE1 channels, from **Fig. 1 – figure supplement 4c-d**), we observe that 70 μM N-AT compensates fairly well (or overcompensates) for the mutation-induced reduction in current amplitude (**Fig. 4g**, **Fig. 4 – figure supplement 4c**). Moreover, for all mutant and wild-type K_V7.1+KCNE1 channels, 70 μM N-AT speeds up the opening kinetics at +40 mV by a factor of 1.3-2.5 (**Supplementary File 3**). 70 μM N-AT also slows down the closing kinetics for most mutants and wild-type K_V7.1+KCNE1 (**Supplementary File 3**). For F351A heterozygous expression and R583C homozygous expression, 70 μM N-AT restores the closing kinetics so that the closing kinetics is not statistically different ($P > 0.05$) from wild-type K_V7.1+KCNE1 closing kinetics (737 ± 62 ms and 833 ± 74 ms, respectively compared to 967 ± 47 ms for wild-type). In the presence of KCNE1, channels made with F193L heterozygous expression, L251A

homozygous expression, and R583C heterozygous expression have wild-type like closing kinetics already before application of N-AT.

N-AT affects both S4 movement and gate opening in mutants

We next use voltage clamp fluorometry on K_V7.1/G219C*/S225L+KCNE1 and K_V7.1/G219C*/F351A+KCNE1 to explore the mechanism by which N-AT enhances the activity of two mechanistically different mutants. Surprisingly, N-AT caused a dramatic decrease in the fluorescence from Alexa488-labeled K_V7.1/G219C*+KCNE1 channels (**Fig. 5 – figure supplement 1a**). In contrast, N-AT did not decrease the fluorescence from Alexa488-labeled K_V7.1/G219C* channels nor from unbound Alexa488 (even up to concentrations of 0.5 M N-AT; **Fig. 5 – figure supplement 1b**), suggesting that N-AT is not a collisional quencher of Alexa488. The mechanism of the N-AT-induced decrease of fluorescence from Alexa488-labeled K_V7.1/G219C*+KCNE1 channels is not clear, but could be due to N-AT inducing a conformational change in KCNE1 or K_V7.1 that brings a quenching residue close to Alexa488.

Due to the dramatic decrease in the fluorescence signal from Alexa488-labeled K_V7.1/G219C*+KCNE1 channels, we have to normalize the $F(V)$ curves obtained in N-AT to the amplitude of the $F(V)$ in control solutions. With this normalization, voltage clamp fluorometry experiments on K_V7.1/G219C*/S225L+KCNE1 indicate that N-AT shifts both the voltage dependence of the first part (which represents $F1$) and the second part (which represents $F2$) of the $F(V)$ curve towards more negative voltages (**Fig. 5 – figure supplement 1c**). However, due to the not completely saturating $F(V)$ for K_V7.1/G219C*/F351A+KCNE1, we are unable to reliably normalize the $F(V)$ curves in the presence of N-AT to the control $F(V)$ curves. We instead explore the effect of N-AT on the kinetics of the two fluorescence

components: *F*1, which is seen as a fast fluorescence change at negative voltages, and *F*2, which is seen as a slow fluorescence change on top of the *F*1 component at positive voltages[24]. *F*1 correlates with the measured gating currents in K_V7.1+KCNE1 channels (and the initial delay in the K_V7.1+KCNE1 ionic currents), whereas *F*2 correlates with the opening of K_V7.1+KCNE1 channels[24]. For both mutants, 70 μM N-AT speeds up *F*1 kinetics (**Fig. 5a**,**d**, measured at –40 mV where virtually no channels open and the fluorescence is mainly composed of *F*1). Numeric values for N-AT effects on channel kinetics are summarized in Figure 5f. Moreover, N-AT accelerates the channel opening kinetics (**Fig. 5b**,**e**) and both the *F1* and *F*2 fluorescence components at +80 mV for K_V7.1/G219C*/S225L+KCNE1 (**Fig. 5f**). The change in the *F2* component is probably larger than what the fits of a double-exponential function suggest, because the slow part of the fluorescence, mainly *F2*, overlay nicely on the currents in both the presence and absence of 70 μM N-AT (**Fig. 5c**, upper panel). As a control, we show that the fluorescence in N-AT does not, however, overlay the currents in control solutions and vice versa (**Fig. 5c**, middle and lower panel). For K_V7.1/G219C*/F351A+KCNE1, the *G*(*V*) curve and the *F*2 component are so shifted towards depolarizing voltages that we cannot reliably quantify the *F*2 component in our fluorescence traces. 70 μM N-AT does, however, speed up K_V7.1/G219C*/F351A+KCNE1 current kinetics (**Fig. 5e**), which suggests that N-AT also speeds up *F*2 in K_V7.1/G219C*/F351A+KCNE1. Altogether, these results suggest that N-AT accelerates both conformational changes during the main gating charge movement and channel opening.

Discussion

We show that all studied LQTS and LQTS-like mutations i) shift the *G*(*V*) of K_V7.1+KCNE1 towards more positive voltages, and/or ii) accelerate K_V7.1+KCNE1 closing. This suggests that at least part of the mechanism underlying the reduced ability of these mutants to generate

K^+ currents is by altering these biophysical properties of the K_V7.1+KCNE1 channel. Using voltage clamp fluorometry in combination with kinetic modeling, we further suggest that these altered biophysical properties in mutants may be caused by interference with different gating transitions. Our experimental data and kinetic modeling are consistent with a model in which K_V7.1/S225L primarily causes reduced channel function by altering the main voltage sensor movement, while K_V7.1/F351A alters later gating transitions associated with pore opening. The different effects of S225L and F351A on the fluorescence *versus* voltage relationships in K_V7.1/G219C* and K_V7.1/G219C*+KCNE1 suggest that these mutations cause channel dysfunction via different molecular mechanisms. Note that we used the LQTS-like F351A mutant, because the LQTS mutant F351S did not generate any currents (Fig. 1 – figure supplement 1). However, during the review process of this manuscript a new LQTS mutant, F351L, was found[35]. The current and fluorescence of this LQTS mutant is very similar to the current and fluorescence of F351A (**Fig. 3 – figure supplement 3**), suggesting that our conclusions on the LQTS-like F351A is also relevant for the LQTS mutant F351L.

One of the mutants, F193L, has only minor effects on the biophysical properties of K_V7.1+KCNE1. This mutant was previously reported to have reduced current amplitude compared to the wild-type K_V7.1+KCNE1 channel and a mild clinical phenotype[13]. The F193L mutation may therefore cause loss of function by faster deactivation kinetics and lower current density. Heterozygous expression of mutated subunits and wild-type subunits in equal molar ratios results in general in a milder biophysical phenotype (more close to the wild-type phenotype). This is in line with a milder clinical phenotype generally reported for heterozygous carriers of LQTS mutations compared to individuals with homozygous genotypes[36-38]. Moreover, for different mutations different biophysical effects of the mutations could be dominant or recessive: For S225L and L251A, heterozygous expression

385 in the presence of KCNE1 partially or completely restores wild-type like V_{50}, whereas
386 heterozygous expression does not improve closing kinetics compared to homozygous
387 expression. For KCNE1/K70N and KCNE1/S74L, co-expression with wild-type KCNE1
388 subunits also restores wild-type like V_{50}, whereas wild-type like closing kinetics is only
389 partially restored. In contrast, for K_V7.1/R583C, heterozygous expression restores wild-type
390 like closing kinetics, but not wild-type like V_{50}. However, because of uncertainties regarding
391 the stoichiometry of mutant to wild-type subunits in assembled K_V7.1+KCNE1 channels (as
392 mentioned in the Results section), further studies will be required to understand the
393 mechanisms underlying these apparent dominant or recessive effects and to evaluate possible
394 physiological impact of these effects.
395
396 Our results show that all tested mutants respond to N-AT. This is in contrast to previously
397 reported K_V7 channel activators on disease-causing K_V7 mutants, for which mutants show
398 markedly different sensitivity[39-41]. 70 µM N-AT shifts the $G(V)$ curve of the wild-type
399 K_V7.1+KCNE1 channel and of all LQTS and LQTS-like mutants by approximately (–50)-(–
400 30) mV, accelerates channel opening and slows down channel closing. In the presence of 70
401 µM N-AT, the V_{50} of all LQTS and LQTS-like mutants are similar to or more negative than
402 V_{50} for the wild-type K_V7.1+KCNE1 channel. For most mutants, 70 µM N-AT
403 overcompensates for the shift in $G(V)$ and reduction in current amplitude caused by the
404 mutations, indicating that a lower N-AT concentration or a less potent N-AT analogue could
405 be used to restore wild-type like $G(V)$ and current amplitudes. Moreover, K_V7.1+KCNE1
406 opening and closing kinetics are partially or completely restored by N-AT. Also, although the
407 disease aetiology of the F193L mutant is likely mainly reduced channel expression, the N-AT
408 induced augmentation caused by a shift in $G(V)$ and increased currents may at least in part
409 overcome the reduction in currents caused by the reduced channel expression. This general

ability of N-AT to, at least partly, compensate for the reduced function of mutants in different parts of the K_V7.1+KCNE1 channel complex and with seemingly different molecular defects, as long as a population of these mutant channels reaches the plasma membrane, suggests that N-AT is an interesting model compound for development of future anti-arrhythmics to treat LQTS caused by diverse K_V7.1+KCNE1 mutations.

Defective trafficking of mutant K_V11.1 ion channels is a common cause of LQTS type 2. About 80-90% of LQTS type 2-associated hERG mutants are estimated to suffer from defective trafficking[42, 43]. The corresponding number for LQTS-associated K_V7.1 and KCNE1 mutants is not clear. Previous studies identify both trafficking defective and trafficking competent K_V7.1 and KCNE1 mutants[e.g. 12, 18, 44]. We are particularly interested to understand the mechanism that underlies abnormal gating of K_V7.1 and KCNE1 mutants. To avoid mutants with severe trafficking defects, we therefore selected mutants that have previously been shown to localize abundantly enough to the cell membrane to generate detectable K^+ currents. Several of the selected mutants have been shown to traffic well in mammalian systems (K_V7.1/V215M and KCNE1/S74L[14, 18]) or generate clearly detectable currents in mammalian cells (K_V7.1/R583C[17]). Our *Xenopus* oocyte experiments that compare mutant current amplitudes with wild-type current amplitudes (**Fig. 1 – figure supplement 4**) suggest that the reduced ability of the selected mutants to generate currents in *Xenopus* oocytes may largely be explained by the shifted $G(V)$ of mutants. Trafficking defects could be disguised in *Xenopus* oocytes that are cultured at low temperatures that may rescue some trafficking defects[42, 45]. These current amplitude experiments should therefore be interpreted with caution until trafficking of specific K_V7.1 and KCNE1 LQTS mutants in mammalian systems has been explored. Previous studies show that membrane expression of trafficking-defect channel mutants (e.g. for K_V11.1 and CFTR) can be pharmacologically

435 rescued using compounds that are suggested to stabilize channel conformation during folding
436 and trafficking[42, 45, 46]. However, rescue of membrane expression may only partially
437 compensate for mutation-induced loss of function, if these mutants also suffer from defective
438 gating[47]. Our proposed N-AT model for pharmacological correction of "*G*(*V*)" LQTS mutants
439 could therefore potentially complement pharmacological correction of trafficking-defect
440 LQTS mutants to improve the outcome of patients suffering from LQTS.
441
442 We previously suggested that polyunsaturated fatty acids and their analogues (such as N-AT)
443 attract the voltage sensor S4 in K_V7.1 by an electrostatic mechanism and thereby shift the
444 *G*(*V*) towards more negative voltages and speed up channel opening[29]. We therefore initially
445 hypothesized that N-AT only would restore the function of those LQTS mutations with
446 altered S4 movement. We were pleasantly surprised when N-AT seems to be able to restore
447 the function of many LQTS and LQTS-like mutants, with diverse mutational defects (such as
448 S225L and F351A). Using voltage clamp fluorometry, we have previously shown that both
449 the main gating charge movement and the gate opening of K_V7.1+KCNE1 channels are
450 accompanied by fluorescence signals from fluorophores attached to S4[24]. This suggests that
451 S4 moves both during the main gating charge movement and during the subsequent channel
452 opening in K_V7.1+KCNE1 channels[24], which is similar to observations in Shaker K_V
453 channels[48-50]. Therefore, N-AT could affect both the main gating charge movement and gate
454 opening by acting on the S4 voltage sensor, as has been shown for hanatoxin which targets
455 the voltage-sensing domain in the Shaker K_V channel[51]. This hypothesis is supported by our
456 voltage-clamp fluorometry experiments using K_V7.1/S225L and K_V7.1/F351A in which N-
457 AT accelerates the fluorescence components associated with both the main S4 movement
458 (*F*1) and gate opening (*F*2), as well as accelerates the kinetics of channel opening. This
459 proposed mechanism would explain why N-AT can restore the function of mutations that

mainly target the main S4 movement or gate opening. However, the dramatic decrease in the fluorescence signal caused by N-AT makes it hard for us to explore the effect of N-AT on the $F(V)$ of mutants. Therefore, the complete mechanism of N-AT in the different mutations is not clear.

Careful future studies are required to assess the clinical utility of PUFA analogues in cardiomyocytes and animal models. We see channel specificity of PUFA analogues as one major challenge and appreciate the need to improve PUFA analogue affinity to K_V7.1+KCNE1 to reduce required therapeutic concentrations and minimize potential adverse effects. Despite these challenges, our data show that the magnitude of N-AT-induced voltage shifts are in the range of shifts induced by several LQTS mutations, and serve as proof of concept that this PUFA analogue, at least partly, restores channel function in diverse LQTS and LQTS-like mutants.

Materials and Methods

Experiments were approved by The Linköping Animal Ethics Committee at Linköping University and The Animal Experiments Inspectorate under the Danish Ministry of Food, Agriculture and Fisheries (University of Copenhagen).

Experiments on Xenopus laevis oocytes

Molecular biology

Expression plasmids human $K_V7.1$ (GenBank Acc.No. NM_000218) in pXOOM and KCNE1 (NM_000219) in pGEM have been previously described[52, 53]. LQTS and LQTS-like point mutations and G219C were introduced into $K_V7.1$ or KCNE1 using site-directed mutagenesis (QuikChange Stratagene, CA, USA). All newly generated constructs were sequenced to ensure integrity (Genewiz, NJ, USA). cRNA was prepared from linearized DNA using the T7 mMessage mMachine transcription kit (Ambion, TX, USA). RNA quality was checked by gel electrophoresis, and RNA concentrations were quantified by UV spectroscopy.

Two-electrode voltage-clamp electrophysiology

Xenopus laevis oocytes (from EcoCyte Bioscience, TX, USA, or prepared in house) were isolated and maintained as previously described[54]. 50 nl cRNA (~50 ng $K_V7.1$ for $K_V7.1$-only expression, 25 ng $K_V7.1$ + 8 ng KCNE1 for homozygous expression, or 12.5 ng $K_V7.1^{wt}$ + 12.5 ng $K_V7.1^{mut}$ + 8 ng $KCNE1^{wt}$ alternatively 25 ng $K_V7.1^{wt}$ + 4 ng $KCNE1^{wt}$ + 4 ng $KCNE1^{mut}$ for heterozygous expression) was injected into each oocyte. Currents were measured at room temperature 2-5 days after injection with the two-electrode voltage-clamp technique (CA-1B amplifier, Dagan, MN, USA). For the current amplitude experiments

presented in **Figure 1- figure supplement 4**, the current amplitude of mutants were normalized to the current amplitude of wild-type K_V7.1+KCNE1 expressed in the same batch of oocytes and incubated under identical conditions for the same time period. Currents were sampled at 1-3.3 kHz, filtered at 500 Hz, and not leakage corrected. The control solution contained (in mM): 88 NaCl, 1 KCl, 15 HEPES, 0.4 $CaCl_2$, and 0.8 $MgCl_2$ (pH adjusted to 7.4 using NaOH). The holding voltage was generally set to −80 mV. Activation curves were generally elicited by stepping to test voltages between −110 and +60 mV (3-5 s durations and 10 mV increments) followed by a tail voltage of −20 mV. Voltage clamp fluorometry experiments were performed as previously described on oocytes labeled for 30 min with 100 µM Alexa-488-maleimide (Molecular Probes) at 4°C[24-26]. For voltage clamp fluorometry experiments on K_V7.1/G219C*, the holding voltage was –80 mV, the pre-pulse –120 mV for 2 s, and test voltages ranging between –140 and +80 mV for 3 s in 20 mV increments. The tail voltage was –80 mV. For K_V7.1/G219C*/KCNE1, the holding voltage was –80 mV, the pre-pulse –160 mV for 5 s, and test voltages ranging between –160 and +80 mV for 5 s in 20 mV increments. The tail voltage was –40 mV. N-arachidonoyl taurine was purchased from Cayman Chemical (MI, USA) and stored, diluted and applied to the oocyte chamber as previously described[29]. Control solution was added to the bath using a gravity-driven perfusion system.

Electrophysiological analysis

To quantify effects on the $G(V)$, tail currents (measured shortly after initiation of tail voltage) were plotted against the pre-pulse (test) voltage. The following Boltzmann relation was fitted to the data

$$G_K(V) = G_{max} / (1 + \exp((V_{50} - V) / s)), \quad (1)$$

where V_{50} is the midpoint (i.e. the voltage at which the conductance is half the maximal conductance estimated from the fit) and *s* the slope factor (shared slope for control and N-AT curves within the same cell). In figures showing I_{tail} *vs* voltage, the curves are normalized to the fitted G_{max}. The same single Boltzmann relation was used to fit the $F(V)$ from voltage clamp fluorometry recordings of $K_V7.1$ without KCNE1 co-expression, where fluorescence at the end of the test pulse was plotted *versus* the test voltage[24]. For voltage-clamp fluorometry recordings of $K_V7.1$ with KCNE1 co-expression (and F351A without KCNE1), a double Boltzmann relation was used[24]. For experiments where conductance or fluorescence did not clearly show signs of saturation in the experimental voltage range, these fits should be considered as an approximation. To estimate the effect of N-AT on Gibbs free energy, the following relation was used:

$$\Delta\Delta G_o = z * \Delta V_{50} * F, \quad (2)$$

Where z is the gating charge of each channel deduced from the slope of the Boltzmann fits according to z = 25/s, ΔV_{50} is the N-AT induced shift in the V_{50} values from the Boltzmann fits, and F is Faraday's constant[55-57]. This analysis assumes a two-state model and tends to underestimate the z[58]. The calculated $\Delta\Delta G_o$ should therefore be seen as an approximation. For opening and closing kinetics, $T_{50,open}$ was defined as the time it takes to reach 50% of the current in the end of a 3 s (5 s for KCNE1 co-expression) long test pulse to +40 mV. $T_{50,close}$ was defined as the time it takes to reduce the amplitude (= instantaneous tail current – steady state tail current) of the tail current by 50% when stepping to a tail pulse to −20 for 5 s. To analyze the effect of N-AT on fluorescence and current kinetics, single or double

exponentials were fitted to the fluorescence or current traces. The ratios of time constants before and after application of N-AT were then calculated.

Modeling

Fluorescence and currents from the $K_V7.1$+KCNE1 models were simulated using Berkeley Madonna (Berkeley, CA).

Statistics

Average values are expressed as mean ± SEM. Mutant parameters (e.g. V_{50} and $\Delta\Delta G_o$) were compared to wild-type parameters using one-way ANOVA with Dunnett's Multiple Comparison Test. Comparison of homozygous and heterozygous expression was done using one-way ANOVA with pair-wise Bonferroni's Test. Effects of N-AT on fluorescence and current kinetics were analysed using two-tailed one sample *t*-test where ratios were compared with a hypothetical value of 1. $P < 0.05$ is considered as statistically significant.

Acknowledgements

We thank Frida Starck Härlin (Linköping University) and Briana Watkins (University of Miami) for help with some experiments and Drs. Fredrik Elinder (Linköping University), Laura Bianchi and Feng Qiu (University of Miami), Nicole Schmitt, Mark Skarsfeldt and Federico Denti (University of Copenhagen) for valuable comments.

Competing Interests

A patent application (62/032,739) based on these results has been submitted by the University of Miami with S.I.L. and H.P.L. identified as inventors.

References

1. Hedley, P.L., Jorgensen, P., Schlamowitz, S., Wangari, R., Moolman-Smook, J., Brink, P.A., Kanters, J.K., Corfield, V.A. & Christiansen, M. The genetic basis of long QT and short QT syndromes: a mutation update. *Hum Mutat* **30,** 1486-1511 (2009).
2. Morita, H., Wu, J. & Zipes, D.P. The QT syndromes: long and short. *Lancet* **372,** 750-763 (2008).
3. Cerrone, M., Cummings, S., Alansari, T. & Priori, S.G. A clinical approach to inherited arrhythmias. *Circ Cardiovasc Genet* **5,** 581-590 (2012).
4. Barhanin, J., Lesage, F., Guillemare, E., Fink, M., Lazdunski, M. & Romey, G. K(V)LQT1 and lsK (minK) proteins associate to form the I(Ks) cardiac potassium current. *Nature* **384,** 78-80 (1996).
5. Sanguinetti, M.C., Curran, M.E., Zou, A., Shen, J., Spector, P.S., Atkinson, D.L. & Keating, M.T. Coassembly of K(V)LQT1 and minK (IsK) proteins to form cardiac I(Ks) potassium channel. *Nature* **384,** 80-83 (1996).
6. Nerbonne, J.M. & Kass, R.S. Molecular physiology of cardiac repolarization. *Physiol Rev* **85,** 1205-1253 (2005).
7. Nakajo, K., Ulbrich, M.H., Kubo, Y. & Isacoff, E.Y. Stoichiometry of the KCNQ1 - KCNE1 ion channel complex. *Proc Natl Acad Sci U S A* **107,** 18862-18867 (2010).
8. Plant, L.D., Xiong, D., Dai, H. & Goldstein, S.A. Individual IKs channels at the surface of mammalian cells contain two KCNE1 accessory subunits. *Proc Natl Acad Sci U S A* **111,** E1438-1446 (2014).
9. Murray, C.I., Westhoff, M., Eldstrom, J., Thompson, E., Emes, R. & Fedida, D. Unnatural amino acid photo-crosslinking of the IKs channel complex demonstrates a KCNE1:KCNQ1 stoichiometry of up to 4:4. *Elife* **5,** e11815 (2016).

10. Liin, S.I., Barro-Soria, R. & Larsson, H.P. The KCNQ1 channel - remarkable flexibility in gating allows for functional versatility. *J Physiol* **593,** 2605-2615 (2015).
11. Nakajo, K. & Kubo, Y. KCNQ1 channel modulation by KCNE proteins via the voltage-sensing domain. *J Physiol* **593,** 2617-2625 (2015).
12. Bianchi, L., Priori, S.G., Napolitano, C., Surewicz, K.A., Dennis, A.T., Memmi, M., Schwartz, P.J. & Brown, A.M. Mechanisms of I(Ks) suppression in LQT1 mutants. *Am J Physiol Heart Circ Physiol* **279,** H3003-3011 (2000).
13. Yamaguchi, M., Shimizu, M., Ino, H., Terai, H., Hayashi, K., Mabuchi, H., Hoshi, N. & Higashida, H. Clinical and electrophysiological characterization of a novel mutation (F193L) in the KCNQ1 gene associated with long QT syndrome. *Clin Sci (Lond)* **104,** 377-382 (2003).
14. Eldstrom, J., Xu, H., Werry, D., Kang, C., Loewen, M.E., Degenhardt, A., Sanatani, S., Tibbits, G.F., Sanders, C. & Fedida, D. Mechanistic basis for LQT1 caused by S3 mutations in the KCNQ1 subunit of IKs. *J Gen Physiol* **135,** 433-448 (2010).
15. Henrion, U., Strutz-Seebohm, N., Duszenko, M., Lang, F. & Seebohm, G. Long QT syndrome-associated mutations in the voltage sensor of I(Ks) channels. *Cell Physiol Biochem* **24,** 11-16 (2009).
16. Yang, T., Smith, J.A., Leake, B.F., Sanders, C.R., Meiler, J. & Roden, D.M. An allosteric mechanism for drug block of the human cardiac potassium channel KCNQ1. *Mol Pharmacol* **83,** 481-489 (2012).
17. Yang, P., Kanki, H., Drolet, B., Yang, T., Wei, J., Viswanathan, P.C., Hohnloser, S.H., Shimizu, W., Schwartz, P.J., Stanton, M., Murray, K.T., Norris, K., George, A.L., Jr. & Roden, D.M. Allelic variants in long-QT disease genes in patients with drug-associated torsades de pointes. *Circulation* **105,** 1943-1948 (2002).

18. Harmer, S.C., Wilson, A.J., Aldridge, R. & Tinker, A. Mechanisms of disease pathogenesis in long QT syndrome type 5. *Am J Physiol Cell Physiol* **298,** C263-273 (2010).

19. Splawski, I., Tristani-Firouzi, M., Lehmann, M.H., Sanguinetti, M.C. & Keating, M.T. Mutations in the hminK gene cause long QT syndrome and suppress IKs function. *Nat Genet* **17,** 338-340 (1997).

20. Priori, S.G., Napolitano, C. & Schwartz, P.J. Low penetrance in the long-QT syndrome: clinical impact. *Circulation* **99,** 529-533 (1999).

21. Napolitano, C., Priori, S.G., Schwartz, P.J., Bloise, R., Ronchetti, E., Nastoli, J., Bottelli, G., Cerrone, M. & Leonardi, S. Genetic testing in the long QT syndrome: development and validation of an efficient approach to genotyping in clinical practice. *Jama* **294,** 2975-2980 (2005).

22. Lai, L.P., Su, Y.N., Hsieh, F.J., Chiang, F.T., Juang, J.M., Liu, Y.B., Ho, Y.L., Chen, W.J., Yeh, S.J., Wang, C.C., Ko, Y.L., Wu, T.J., Ueng, K.C., Lei, M.H., Tsao, H.M., Chen, S.A., Lin, T.K., Wu, M.H., Lo, H.M., Huang, S.K. & Lin, J.L. Denaturing high-performance liquid chromatography screening of the long QT syndrome-related cardiac sodium and potassium channel genes and identification of novel mutations and single nucleotide polymorphisms. *J Hum Genet* **50,** 490-496 (2005).

23. Deschenes, D., Acharfi, S., Pouliot, V., Hegele, R., Krahn, A., Daleau, P. & Chahine, M. Biophysical characteristics of a new mutation on the KCNQ1 potassium channel (L251P) causing long QT syndrome. *Can J Physiol Pharmacol* **81,** 129-134 (2003).

24. Barro-Soria, R., Rebolledo, S., Liin, S.I., Perez, M.E., Sampson, K.J., Kass, R.S. & Larsson, H.P. KCNE1 divides the voltage sensor movement in KCNQ1/KCNE1 channels into two steps. *Nat Commun* **5,** 3750 (2014).

25. Osteen, J.D., Gonzalez, C., Sampson, K.J., Iyer, V., Rebolledo, S., Larsson, H.P. & Kass, R.S. KCNE1 alters the voltage sensor movements necessary to open the KCNQ1 channel gate. *Proc Natl Acad Sci U S A* **107,** 22710-22715 (2010).

26. Osteen, J.D., Barro-Soria, R., Robey, S., Sampson, K.J., Kass, R.S. & Larsson, H.P. Allosteric gating mechanism underlies the flexible gating of KCNQ1 potassium channels. *Proc Natl Acad Sci U S A* **109,** 7103-7108 (2012).

27. Zaydman, M.A., Kasimova, M.A., McFarland, K., Beller, Z., Hou, P., Kinser, H.E., Liang, H., Zhang, G., Shi, J., Tarek, M. & Cui, J. Domain-domain interactions determine the gating, permeation, pharmacology, and subunit modulation of the IKs ion channel. *Elife* **3,** e03606 (2014).

28. Ruscic, K.J., Miceli, F., Villalba-Galea, C.A., Dai, H., Mishina, Y., Bezanilla, F. & Goldstein, S.A. IKs channels open slowly because KCNE1 accessory subunits slow the movement of S4 voltage sensors in KCNQ1 pore-forming subunits. *Proc Natl Acad Sci U S A* **110,** E559-566 (2013).

29. Liin, S.I., Silvera Ejneby, M., Barro-Soria, R., Skarsfeldt, M.A., Larsson, J.E., Starck Harlin, F., Parkkari, T., Bentzen, B.H., Schmitt, N., Larsson, H.P. & Elinder, F. Polyunsaturated fatty acid analogs act antiarrhythmically on the cardiac IKs channel. *Proc Natl Acad Sci U S A* **112,** 5714-5719 (2015).

30. O'Hara, T., Virag, L., Varro, A. & Rudy, Y. Simulation of the undiseased human cardiac ventricular action potential: model formulation and experimental validation. *PLoS Comput Biol* **7,** e1002061 (2011).

31. Piacentino, V., 3rd, Weber, C.R., Chen, X., Weisser-Thomas, J., Margulies, K.B., Bers, D.M. & Houser, S.R. Cellular basis of abnormal calcium transients of failing human ventricular myocytes. *Circ Res* **92,** 651-658 (2003).

32. Silva, J. & Rudy, Y. Subunit interaction determines IKs participation in cardiac repolarization and repolarization reserve. *Circulation* **112,** 1384-1391 (2005).
33. Busch, A.E. & Lang, F. Effects of [Ca2+]i and temperature on minK channels expressed in Xenopus oocytes. *FEBS Lett* **334,** 221-224 (1993).
34. Seebohm, G., Lerche, C., Busch, A.E. & Bachmann, A. Dependence of I(Ks) biophysical properties on the expression system. *Pflugers Arch* **442,** 891-895 (2001).
35. Vyas, B., Puri, R.D., Namboodiri, N., Saxena, R., Nair, M., Balakrishnan, P., Jayakrishnan, M.P., Udyavar, A., Kishore, R. & Verma, I.C. Phenotype guided characterization and molecular analysis of Indian patients with long QT syndromes. *Indian Pacing Electrophysiol J* **16,** 8-18 (2016).
36. Priori, S.G., Schwartz, P.J., Napolitano, C., Bianchi, L., Dennis, A., De Fusco, M., Brown, A.M. & Casari, G. A recessive variant of the Romano-Ward long-QT syndrome? *Circulation* **97,** 2420-2425 (1998).
37. Jackson, H.A., McIntosh, S., Whittome, B., Asuri, S., Casey, B., Kerr, C., Tang, A. & Arbour, L.T. LQTS in Northern BC: homozygosity for KCNQ1 V205M presents with a more severe cardiac phenotype but with minimal impact on auditory function. *Clin Genet* **86,** 85-90 (2014).
38. Zhang, S., Yin, K., Ren, X., Wang, P., Zhang, S., Cheng, L., Yang, J., Liu, J.Y., Liu, M. & Wang, Q.K. Identification of a novel KCNQ1 mutation associated with both Jervell and Lange-Nielsen and Romano-Ward forms of long QT syndrome in a Chinese family. *BMC Med Genet* **9,** 24 (2008).
39. Seebohm, G., Pusch, M., Chen, J. & Sanguinetti, M.C. Pharmacological activation of normal and arrhythmia-associated mutant KCNQ1 potassium channels. *Circ Res* **93,** 941-947 (2003).

40. Xiong, Q., Sun, H. & Li, M. Zinc pyrithione-mediated activation of voltage-gated KCNQ potassium channels rescues epileptogenic mutants. *Nat Chem Biol* **3,** 287-296 (2007).

41. Leitner, M.G., Feuer, A., Ebers, O., Schreiber, D.N., Halaszovich, C.R. & Oliver, D. Restoration of ion channel function in deafness-causing KCNQ4 mutants by synthetic channel openers. *Br J Pharmacol* **165,** 2244-2259 (2012).

42. Anderson, C.L., Kuzmicki, C.E., Childs, R.R., Hintz, C.J., Delisle, B.P. & January, C.T. Large-scale mutational analysis of Kv11.1 reveals molecular insights into type 2 long QT syndrome. *Nat Commun* **5,** 5535 (2014).

43. Sanguinetti, M.C. HERG1 channelopathies. *Pflugers Arch* **460,** 265-276 (2010).

44. Wilson, A.J., Quinn, K.V., Graves, F.M., Bitner-Glindzicz, M. & Tinker, A. Abnormal KCNQ1 trafficking influences disease pathogenesis in hereditary long QT syndromes (LQT1). *Cardiovasc Res* **67,** 476-486 (2005).

45. Delisle, B.P., Anson, B.D., Rajamani, S. & January, C.T. Biology of cardiac arrhythmias: ion channel protein trafficking. *Circ Res* **94,** 1418-1428 (2004).

46. Sato, S., Ward, C.L., Krouse, M.E., Wine, J.J. & Kopito, R.R. Glycerol reverses the misfolding phenotype of the most common cystic fibrosis mutation. *J Biol Chem* **271,** 635-638 (1996).

47. Perry, M.D., Ng, C.A., Phan, K., David, E., Steer, K., Hunter, M.J., Mann, S.A., Imtiaz, M., Hill, A.P., Ke, Y. & Vandenberg, J.I. Rescue of protein expression defects may not be enough to abolish the pro-arrhythmic phenotype of long QT type 2 mutations. *J Physiol* **594,** 4031-4049 (2016).

48. Börjesson, S.I. & Elinder, F. An electrostatic potassium channel opener targeting the final voltage sensor transition. *J Gen Physiol* **137,** 563-577 (2011).

49. Pathak, M., Kurtz, L., Tombola, F. & Isacoff, E. The cooperative voltage sensor motion that gates a potassium channel. *J Gen Physiol* **125,** 57-69 (2005).

50. Phillips, L.R. & Swartz, K.J. Position and motions of the S4 helix during opening of the Shaker potassium channel. *J Gen Physiol* **136,** 629-644 (2010).

51. Milescu, M., Lee, H.C., Bae, C.H., Kim, J.I. & Swartz, K.J. Opening the shaker K+ channel with hanatoxin. *J Gen Physiol* **141,** 203-216 (2013).

52. Jespersen, T., Grunnet, M., Angelo, K., Klaerke, D.A. & Olesen, S.P. Dual-function vector for protein expression in both mammalian cells and Xenopus laevis oocytes. *Biotechniques* **32,** 536-538, 540 (2002).

53. Schmitt, N., Calloe, K., Nielsen, N.H., Buschmann, M., Speckmann, E.J., Schulze-Bahr, E. & Schwarz, M. The novel C-terminal KCNQ1 mutation M520R alters protein trafficking. *Biochem Biophys Res Commun* **358,** 304-310 (2007).

54. Börjesson, S.I., Parkkari, T., Hammarström, S. & Elinder, F. Electrostatic Tuning of Cellular Excitability. *Biophys J* **98,** 396-403 (2010).

55. Li-Smerin, Y. & Swartz, K.J. Helical structure of the COOH terminus of S3 and its contribution to the gating modifier toxin receptor in voltage-gated ion channels. *J Gen Physiol* **117,** 205-218 (2001).

56. Monks, S.A., Needleman, D.J. & Miller, C. Helical structure and packing orientation of the S2 segment in the Shaker K+ channel. *J Gen Physiol* **113,** 415-423 (1999).

57. DeCaen, P.G., Yarov-Yarovoy, V., Zhao, Y., Scheuer, T. & Catterall, W.A. Disulfide locking a sodium channel voltage sensor reveals ion pair formation during activation. *Proc Natl Acad Sci U S A* **105,** 15142-15147 (2008).

58. Chowdhury, S. & Chanda, B. Estimating the voltage-dependent free energy change of ion channels using the median voltage for activation. *J Gen Physiol* **139,** 3-17 (2011).

750

751

Figure legends

Figure 1. Biophysical properties of LQTS and LQTS-like K_V7.1+KCNE1 channel mutants expressed in *Xenopus* oocytes. (a) Topology of K_V7.1 and KCNE1, and position of tested LQTS and LQTS-like mutants. (b) $G(V)$ midpoints (V_{50}) from the Boltzmann fits for mutants co-expressed with KCNE1. n = 5-11. Data as mean ± SEM. Statistics represent one-way ANOVA with Dunnett's Multiple Comparison Test to compare mutants to wild-type K_V7.1+KCNE1; **P < 0.01; ns is P ≥ 0.05. # denotes lowest estimate. Dashed line denotes wild-type V_{50}. (c) Representative example of K_V7.1/S225L+KCNE1 $G(V)$ (black line and symbols) compared to wild-type K_V7.1+KCNE1 (blue line and symbols, mean ± SEM, n = 5). (d-e) Representative example of K_V7.1/S225L+KCNE1 opening kinetics and K_V7.1+KCNE1/K70N closing kinetics (black lines) compared to wild-type K_V7.1+KCNE1 (blue lines). The following figure supplements are available for figure 1: figure supplement 1, figure supplement 2, figure supplement 3, figure supplement 4.

Figure 2. Comparison of homozygous and heterozygous expression of LQTS and LQTS-like mutants. (a-b) Representative example of kinetics (middle panel) and $G(V)$ (right panel) for homozygous expression and heterozygous expression of S225L (a) and K70N (b). Currents in response to steps from –80 mV to +40 mV (a, middle pane) and from +40 mV to –20 mV (b, middle panel). Homozygous expression (black), heterozygous expression (gray), and K_V7.1+KCNE1 wild-type (blue). n = 7-13. (c-d) Summary of V_{50} (c) and T_{50} for closing (d) for homozygous and heterozygous expression. Data as mean ± SEM. n = 5-13. Statistics represent one-way ANOVA with pair-wise Bonferroni's Test to compare homozygous and heterozygous expression; **P < 0.01; ***P < 0.001; ns is P ≥ 0.05. # denotes lowest estimate. Not determined (nd). Statistics was not calculated for F351A. Dashed lines denote corresponding values for wild-type K_V7.1+KCNE1.

Figure 3. Voltage-clamp fluorometry recordings of wild-type and mutated K_V7.1+KCNE1 channels. (a-c) Representative fluorescence traces and mean *F*(*V*)/*G*(*V*) curves for K_V7.1/G219C* (a), S225L (b), and F351A (c). Left panels without KCNE1 and right panels with KCNE1. The holding voltage is –80 mV, the pre-pulse –120 mV for 2 s (left panels) and –160 mV for 5 s (right panels), and test voltages between –140 and +80 mV for 3 s (left panels) and between –160 and +80 mV for 5 s (right panels) in 20 mV increments. The tail voltage is –80 mV (left panels) and -40 mV (right panels). For K_V7.1/G219C*/F351A+KCNE1, the pre-pulse is –120 mV for 3 s, and test voltages ranging between –160 and +100 mV. The bottom of the fit of the K_V7.1/G219C*/S225L+KCNE1 *F*(*V*) curve (which saturates fairly well at negative voltages) is set to 0 in the normalized *F*(*V*) curves in the right panels. The *F*1 amplitude of K_V7.1/G219C*/F351A+KCNE1 is normalized to the *F*1 amplitude of wild-type. Data as mean ± SEM. *n* = 4-14. The dashed lines in (b) and (c) denote *F*(*V*) (red) and *G*(*V*) (black) for wild-type (from a). The following figure supplements are available for figure 3: figure supplement 1, figure supplement 2, figure supplement 3.

Figure 4. Effect of N-AT on LQTS and LQTS-like mutants. All these experiments are done in the presence of KCNE1. Structure of N-AT is shown. (a-b) Representative effect of 7-70 μM N-AT on current amplitude (a) and *G*(*V*) (b) of K_V7.1/S225L+KCNE1. Dashed line in (a) denotes 0 μA. (c) Representative currents generated by K_V7.1/S225L+KCNE1 during pulsing at 1 Hz and +28°C in control solution (black) and after the cell had been bathed continuously in 70 μM N-AT (light to dark green, # denotes sweep order). Inset: corresponding currents from wild-type K_V7.1+KCNE1 scaled similarly as K_V7.1/S225L+KCNE1. Light grey trace denotes sweep #1, grey trace denotes sweep #2, and

dark grey trace denotes sweep #20. (d) Summary of V_{50} for LQTS and LQTS-like mutants before and after 70 µM N-AT application. Dashed line denotes V_{50} for wild-type K_V7.1+KCNE1. (e-f) Summary of ΔV_{50} (e) and $\Delta\Delta G_o$ (f) for LQTS and LQTS-like mutants induced by 70 µM N-AT. # denotes an approximation. Dashed lines denote corresponding ΔV_{50} and $\Delta\Delta G_o$ induced by 70 µM N-AT for wild-type K_V7.1+KCNE1. Statistics in (f) represent one-way ANOVA with Dunnett's Multiple Comparison Test to compare the N-AT-induced change in $\Delta\Delta G_o$ of mutants to N-AT-induced change in $\Delta\Delta G_o$ of wild-type K_V7.1+KCNE1; *P ≤ 0.05. Only significant differences shown in (f), other comparisons have P > 0.05. (g) Estimate of the ability of 70 µM N-AT to restore LQTS and LQTS-like mutant current amplitude at +40 mV. The mean N-AT induced increase in current amplitude for each mutant (from Figure 4 – figure supplement 4b) is multiplied with the control amplitude for each mutant (from Figure 1 – figure supplement 4d). Not determined (nd). Data as mean ± SEM. n = 5-12. Dashed line denotes relative wild-type K_V7.1+KCNE1 current amplitude in control solution (i.e. without N-AT). The following figure supplements are available for figure 4: figure supplement 1, figure supplement 2, figure supplement 3, figure supplement 4.

Figure 5. Effect of 70 µM N-AT on S4 movement and gate opening in S225L and F351A mutants. (a-c) Representative example of effect of 70 µM N-AT on *F*1 kinetics (a), current opening kinetics (b), and *F*2 kinetics (c) in K_V7.1/G219C*/S225L+KCNE1. Control fluorescence (red) and current (black). N-AT fluorescence (magenta) and current (green). Top in (c) shows overlay of the later part of the fluorescence (after most of *F*1 has occurred) and the later part of the currents (after the initial delay) before and after application of N-AT. Middle and lower (c) show that there is not a great overlap of the fluorescence in the presence of N-AT and the current in control solution (middle) or the fluorescence in control solution and the current in the presence of N-AT (lower). (d-e) Representative example of effect of 70

μM N-AT on *F*1 kinetics (d) and current opening kinetics (e) in K_V7.1/G219C*/F351A+KCNE1. Same colouring as in (a-b). Dashed line in (b) and (e) denotes 0 μA. Fluorescence traces and all traces in (c) have been normalized to better allow temporal comparison. (f) Summary of the effect of 70 μM N-AT on kinetic parameters of K_V7.1/G219C*/S225L+KCNE1 and K_V7.1/G219C*/F351A+KCNE1. Kinetics of the fast (*F*1) and slow (*F*2) fluorescence components were deduced from a double-exponential function fitted to the fluorescence traces. Kinetics of currents were deduced from a single-exponential function fitted to current traces. Ratios of time constants ($\tau_{N\text{-}AT}/\tau_{Ctrl}$) were calculated pair-wise (control compared to N-AT) in each oocyte and analysed using two-tailed one sample *t*-test where ratios were compared with a hypothetical value of 1. Data as mean ± SEM. $n = 4$ (3 for fluorescence kinetics for K_V7.1/G219C*/F351A+KCNE1). *P < 0.05; **P < 0.01. nd = not determined. The following figure supplement is available for figure 5: figure supplement 1.

Figure 1 – figure supplement 1. K_V7.1/F351S mutant expressed in *Xenopus* oocytes. The K_V7.1/F351S mutant does not generate currents when expressed in *Xenopus* oocytes. The holding voltage is –80 mV, and test voltages range between –80 and +60 mV for 3 s in 10 mV increments. The tail voltage is –20 mV.

Figure 1 – figure supplement 2. V_{50} of LQTS and LQTS-like K_V7.1 mutants expressed in *Xenopus* oocytes. *G*(*V*) midpoints (V_{50}) for LQTS and LQTS-like mutants without co-expression of KCNE1. Mean ± SEM. $n = 5\text{-}12$. Statistics represent one-way ANOVA with Dunnett's Multiple Comparison Test to compare V_{50} of mutant to V_{50} of wild-type K_V7.1; **P < 0.01; ns P ≥ 0.05. Dashed line denotes wild-type V_{50}.

Figure 1 – figure supplement 3. K_V7.1/R583C mutant expressed in *Xenopus* oocytes. (a) The K_V7.1/R583C mutant generates currents that inactivate at positive voltages. The holding voltage is –80 mV, and test voltages range between –80 and +40 mV for 3 s in 20 mV increments. The tail voltage is –20 mV. Tail currents are measured at the arrow. Inset: representative current trace at +40 mV for wild-type K_V7.1. (b) Representative example of $G(V)$ curves generated using the protocol in panel a (filled circles) or a triple pulse protocol (open circles) with a brief hyperpolarizing pulse (–140 mV for 20 ms) between the test pulse and the tail pulse to release a fraction of channels from inactivation. The triple pulse protocol generates a $G(V)$ that is shifted ~9 mV towards positive voltages (V_{50} = ~ –39 mV for the regular protocol and –30 mV for the triple pulse protocol), which matches the $G(V)$ of the wild-type K_V7.1 fairly well (V_{50} = –29.4 mV).

Figure 1 – figure supplement 4. Comparison of current amplitude of wild-type K_V7.1+KCNE1 and LQTS and LQTS-like mutants when expressed in *Xenopus* oocytes. K_V7.1 and KCNE1 were co-injected in oocytes for homozygous (a) and heterozygous (b) expression, as described in Materials and Methods. Current were recorded after 2 days of incubation at 16°C. The holding voltage is –80 mV, and test voltages range between 0 and +60 mV for 5 s in 20 mV increments. The tail voltage is –20 mV. Current amplitudes at the end of the 5 s test pulse are normalized to the wild-type K_V7.1+KCNE1 current amplitude at +60 mV recorded in the same batch of oocytes. Dashed line in (a) is the wild-type curve shifted +25 mV. (c-d) Detailed comparison of current amplitudes at +20 mV (c) and +40 mV (d). Mutant current amplitudes are normalized to the wild-type K_V7.1+KCNE1 current amplitude at indicated voltage. Dashed lines denote relative wild-type K_V7.1+KCNE1 current amplitude (= 1). Statistics represent one-way ANOVA with Dunnett's Multiple Comparison

876 Test to compare current amplitude of mutants to wild-type current amplitudes. *P < 0.05; **P
877 < 0.01; ***P < 0.001; ns is P ≥ 0.05. Mean ± SEM. *n* = 4-12.
878
879 **Figure 3 - figure supplement 1. Kinetic models for K_V7.1 and K_V7.1+KCNE1 channel**
880 **gating.** (a) A 10-state allosteric gating scheme for K_V7.1 channels. Horizontal transitions
881 represent independent S4 movements that increase the fluorescence to an intermediate level
882 (which generates the *F*1 component). The vertical transition represents concerted channel
883 opening with a concomitant additional fluorescence increase (which generates the *F*2
884 component). Cartoon shows K_V7.1 channel labeled with a fluorophore on S3-S4 with all four
885 voltage sensors in the resting state (C_0), with one (C_1), or four (C_4) voltage sensor activated in
886 the closed channel (top) or with all four voltage sensors in the resting state (O_0), with one
887 (O_1), or four (O_4) voltage sensor activated with the channel opened (bottom). (b) A 6-state
888 allosteric gating scheme for K_V7.1+KCNE1 channels. Horizontal transitions represent
889 independent S4 movements that increase the fluorescence to an intermediate level (which
890 generates the *F*1 component). The vertical transition represents concerted channel opening
891 with a concomitant additional fluorescence increase (which generates the *F*2 component).
892 Cartoon shows K_V7.1 channel labeled with a fluorophore on S3-S4 with all four voltage
893 sensors in the resting state (C_0), with one (C_1), or four (C_4) voltage sensor activated without
894 channel opening (top) that is followed by a concerted conformational change of all four S4s
895 associated with channel opening (O_4) (bottom).
896
897 **Figure 3 - figure supplement 2. Simulations of wild-type and mutant K_V7.1 and**
898 **K_V7.1+KCNE1 channels reproduce currents and fluorescence.** Simulated *G*(*V*) (black)
899 and *F*(*V*) (red) curves for (a) wild-type, (b) S225L, and (c) F351A K_V7.1 (left) and
900 K_V7.1+KCNE1 (right) channels using the K_V7.1 and K_V7.1+KCNE1 models in Figure 3 -

figure supplement 1. Parameters for the wild-type models were determined in earlier studies (see Supplementary File 4 for all rate constants). Current and fluorescence traces were simulated using Berkeley Madonna (Berkeley, CA).

Figure 3 – figure supplement 3. Voltage-clamp fluorometry recordings of the K_V7.1/G219C*/F351L mutant with and without KCNE1 co-expressed. Mean $F(V)/G(V)$ curves for K_V7.1/G219C*/F351L (mean ± SEM) are shown together with corresponding mean $F(V)/G(V)$ curves for WT K_V7.1/G219C* (blue lines) and K_V7.1/G219C*/F351A (dashed red/black lines). Experiments are performed and data normalized as described in Figure 3. Note that all data presented in this graph are done on constructs with a Kv7.1/C214A/C331A background (Barro-Soria *et al*., 2014[24]; Barro-Soria *et al.*, 2015[59]). The $F(V)/G(V)$ curves are therefore shifted towards negative voltages compared the data presented in Figure 3 (which are done in WT background). n = 4-6.

24. Barro-Soria, R., Rebolledo, S., Liin, S.I., Perez, M.E., Sampson, K.J., Kass, R.S. & Larsson, H.P. KCNE1 divides the voltage sensor movement in KCNQ1/KCNE1 channels into two steps. *Nat Commun* **5,** 3750 (2014).

59. Barro-Soria, R., Perez, M.E. & Larsson, H.P. KCNE3 acts by promoting voltage sensor activation in KCNQ1. *Proc Natl Acad Sci U S A* **112,** E7286-7292 (2015).

Figure 4 – figure supplement 1. N-AT effect on wild-type K_V7.1+KCNE1 expressed in *Xenopus* oocytes. Representative effect of 70 µM N-AT on current amplitude (a) and $G(V)$ (b) of wild-type K_V7.1+KCNE1. The holding voltage is –80 mV and the tail current amplitude in (b) measured at –20 mV after 5 s test pulses. Dashed line in (a) denotes 0 µA current. $G(V)$ curves in (b) are normalized to the fitted G_{max} (as described in Materials and Methods).

Figure 4 – figure supplement 2. Time course of N-AT wash-in on K_V7.1/S225L+KCNE1 expressed in *Xenopus* oocytes. Representative example showing that N-AT effects on current amplitude reaches steady state for each concentration within minutes. The holding voltage is –80 mV and current amplitude measured at the end of a 5 s test pulse to +20 mV. Dashed line denotes baseline (control amplitude).

Figure 4 – figure supplement 3. 'Leak' component of K_V7.1/S225L+KCNE1. Currents generated by the K_V7.1/S225L+KCNE1 mutant have a small instantaneous 'leak' component at positive voltages. Dashed line denotes 0 μA.

Figure 4 – figure supplement 4. Effect of N-AT on current amplitude of LQTS and LQTS-like mutants. (a-b) Current amplitudes in the presence of 70 μM N-AT measured at the end of a 5 s test pulse to +20 mV (a) or +40 mV (b). The currents are normalized to the current amplitude in control solution in the same oocyte. Dashed lines denote N-AT effects on wild-type K_V7.1+KCNE1 current amplitude (a factor 2.9 ± 0.4 and 1.9 ± 0.3 (n = 5), respectively). (c) Ability of 70 μM N-AT to restore LQTS and LQTS-like mutant current amplitude at +20 mV. The mean N-AT-induced fold increase in current amplitude for each mutant (data from panel a) is multiplied by the relative current amplitude for each mutant compared to wild-type K_V7.1+KCNE1 in control solution (from Figure 1 – figure supplement 4). Dashed line denotes relative wild-type K_V7.1+KCNE1 current amplitude in control solution (i.e. without N-AT). Mean ± SEM. n = 4-12. nd = not determined.

Figure 5 – figure supplement 1. Effect of N-AT on the $F(V)$ of K_V7.1/G219C*/S225L mutant co-expressed with KCNE1 in *Xenopus* oocytes. (a) Representative example of the

time course of the reduction in fluorescence intensity upon N-AT application. The fluorescence intensities shown is the fluorescence measured at +80 mV (during repeated applications of the voltage protocol used to measure the complete $F(V)$ as in panel c), normalized to the fluorescence intensity at +80 mV recorded in the first $F(V)$ in control solution. Red symbols denote control (without N-AT) and purple symbols denote in the presence of N-AT. The fluorescence signal reduces with time in the presence of N-AT. In contrast, the fluorescence signal is preserved in the absence of N-AT (red symbol, recorded in another cell). (b) Summary of fluorescence emission monitored from unbound Alexa488 in control solution and in N-AT-supplemented control solution (0.25 or 0.5 M N-AT). In these experiments, no oocytes or channels were present. A.U. denotes arbitrary units. Data as mean ± SEM. $n = 3$. (c) Mean $F(V)$ curve for $K_V7.1$/G219C*/S225L+KCNE1 in the absence (red symbols, data from Figure 3B) or presence of 70 μM N-AT. The holding voltage is –80 mV, the pre-pulse –160 mV for 5 s, and test voltages between –160 and +100 mV for 5 s in 20 mV increments. The tail voltage is –40 mV. Each $F(V)$ curve is normalized between 0 and 1 based on the bottom and top deduced from the double Boltzmann fits for each curve (see Methods). Data as mean ± SEM. $n = 3$ for N-AT.

List of figure supplements and supplementary files

Figure 1 – figure supplement 1

Figure 1 – figure supplement 2

Figure 1 – figure supplement 3

Figure 1 – figure supplement 4

Figure 3 – figure supplement 1

Figure 3 – figure supplement 2

Figure 3 – figure supplement 3

Figure 4 – figure supplement 1

Figure 4 – figure supplement 2

Figure 4 – figure supplement 3

Figure 4 – figure supplement 4

Figure 5 – figure supplement 1

Supplementary File 1

Supplementary File 2

Supplementary File 3

Supplementary File 4

Figure 1

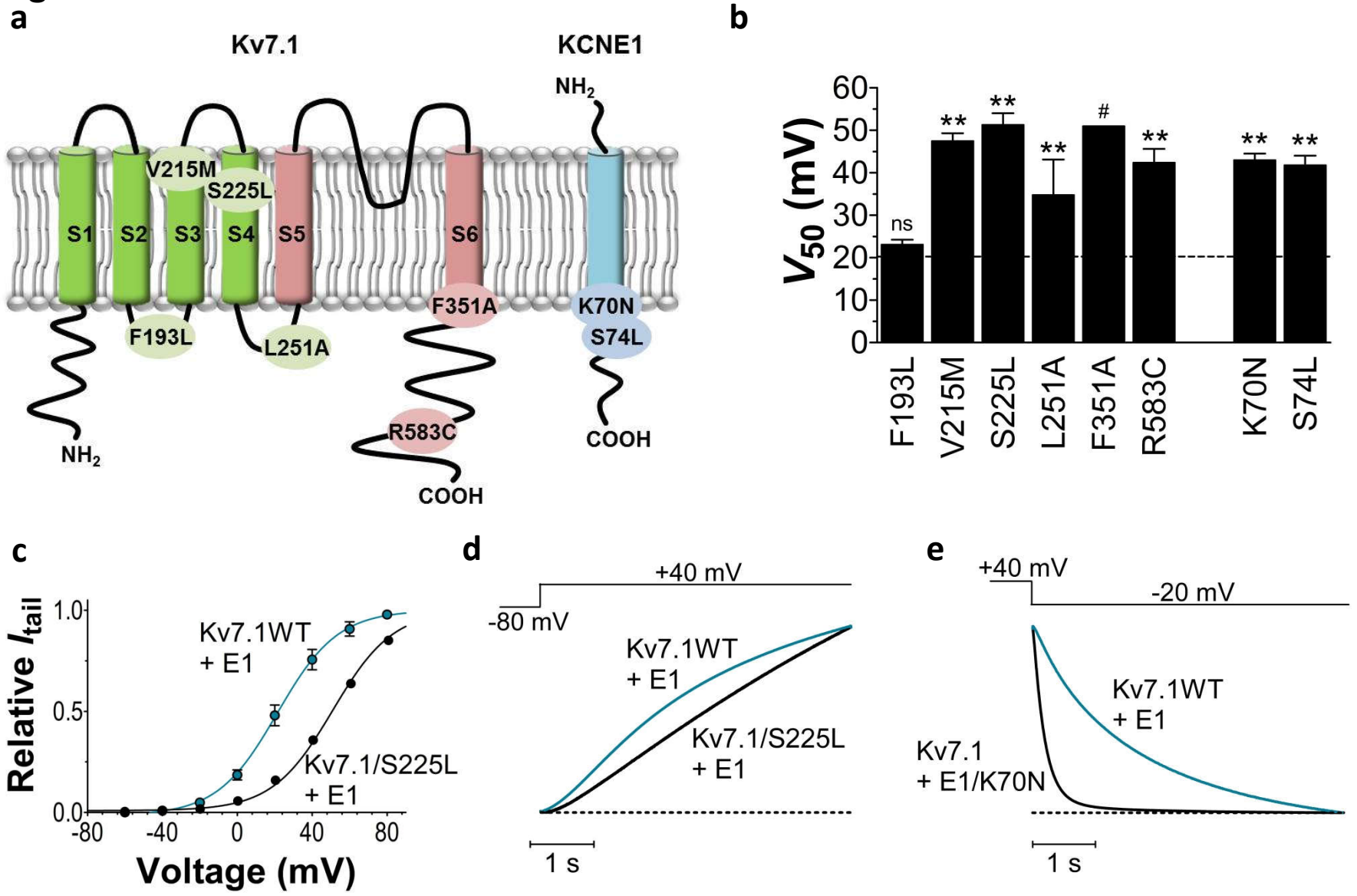
a
Kv7.1
KCNE1
NH2
V215M
S225L
S1
S2
S3
S4
S5
S6
F351A
K70N
S74L
F193L
L251A
R583C
NH2
COOH
COOH
b
V50 (mV)
60
50
40
30
20
10
0
ns
**
**
**
#
**
**
**
F193L
V215M
S225L
L251A
F351A
R583C
K70N
S74L
c
Relative Itail
1.0
0.5
0.0
-80
-40
0
40
80
Voltage (mV)
Kv7.1WT
+ E1
Kv7.1/S225L
+ E1
d
+40 mV
-80 mV
Kv7.1WT
+ E1
Kv7.1/S225L
+ E1
1 s
e
+40 mV
-20 mV
Kv7.1WT
+ E1
Kv7.1
+ E1/K70N
1 s

Figure 2

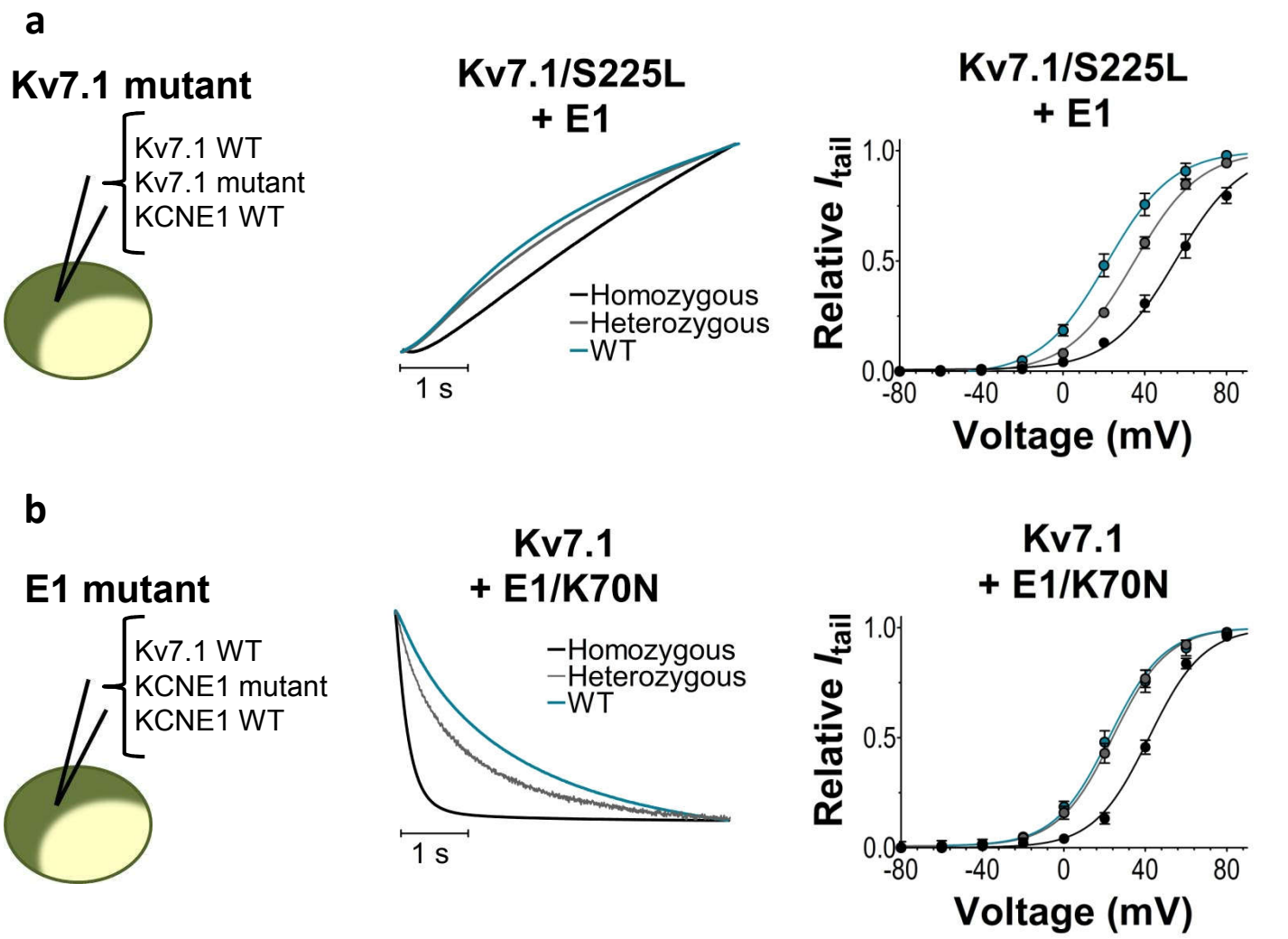
a
Kv7.1 mutant
Kv7.1 WT
Kv7.1 mutant
KCNE1 WT
Kv7.1/S225L
+ E1
Homozygous
Heterozygous
WT
1 s
Kv7.1/S225L
+ E1
Relative I_{tail}
Voltage (mV)
b
E1 mutant
Kv7.1 WT
KCNE1 mutant
KCNE1 WT
Kv7.1
+ E1/K70N
Homozygous
Heterozygous
WT
1 s
Kv7.1
+ E1/K70N
Relative I_{tail}
Voltage (mV)

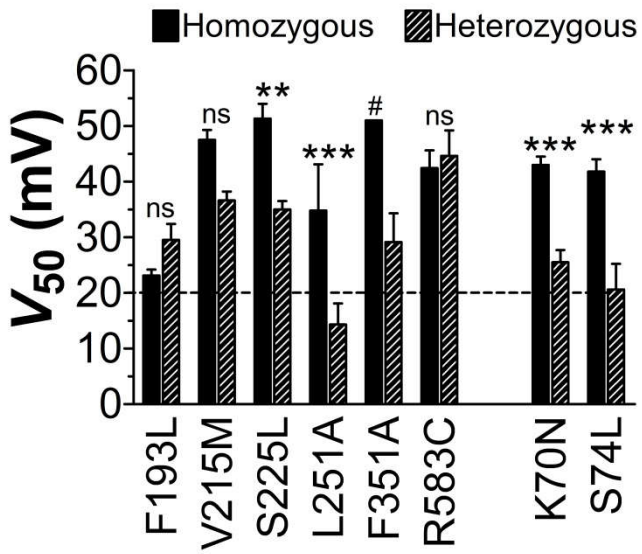
c
Homozygous
Heterozygous
V_{50} (mV)
F193L
V215M
S225L
L251A
F351A
R583C
K70N
S74L

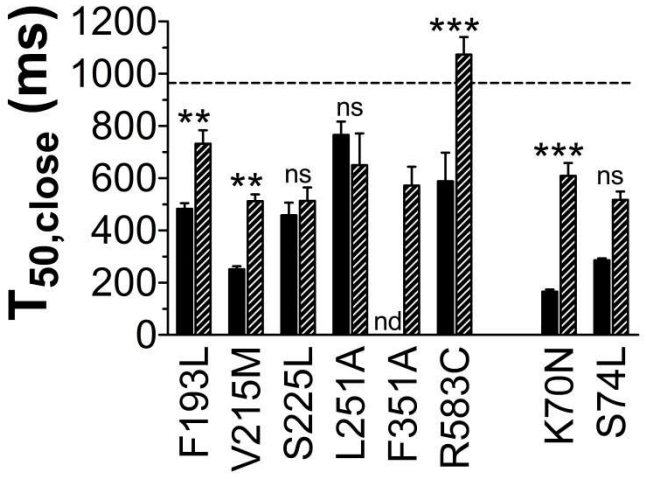
d
$T_{50,close}$ (ms)
nd
F193L
V215M
S225L
L251A
F351A
R583C
K70N
S74L

Figure 3

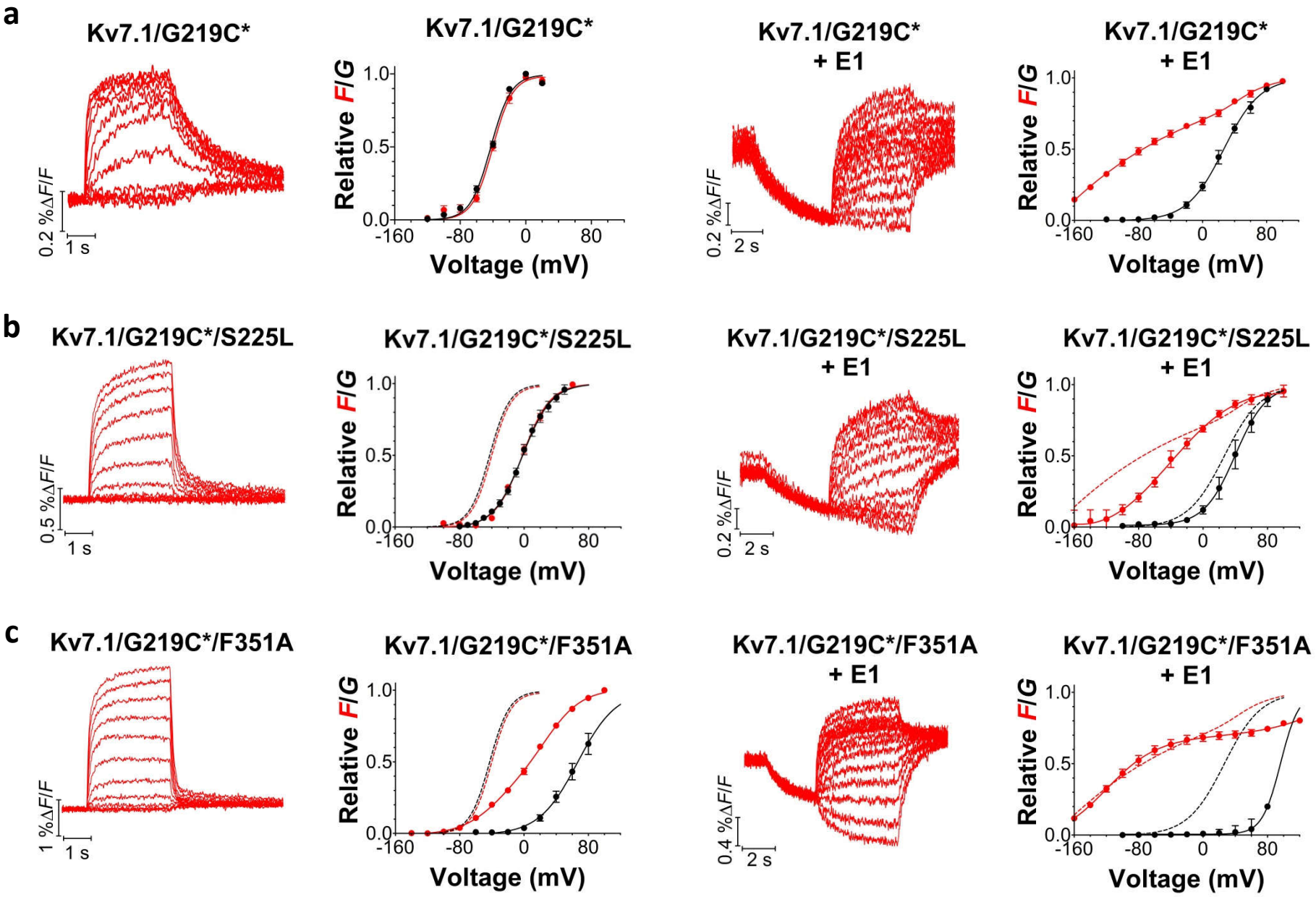
a
Kv7.1/G219C*
0.2 %ΔF/F
1 s
Kv7.1/G219C*
Relative F/G
1.0
0.5
0.0
-160
-80
0
80
Voltage (mV)
Kv7.1/G219C*
+ E1
0.2 %ΔF/F
2 s
Kv7.1/G219C*
+ E1
Relative F/G
1.0
0.5
0.0
-160
-80
0
80
Voltage (mV)
b
Kv7.1/G219C*/S225L
0.5 %ΔF/F
1 s
Kv7.1/G219C*/S225L
Relative F/G
1.0
0.5
0.0
-160
-80
0
80
Voltage (mV)
Kv7.1/G219C*/S225L
+ E1
0.2 %ΔF/F
2 s
Kv7.1/G219C*/S225L
+ E1
Relative F/G
1.0
0.5
0.0
-160
-80
0
80
Voltage (mV)
c
Kv7.1/G219C*/F351A
1 %ΔF/F
1 s
Kv7.1/G219C*/F351A
Relative F/G
1.0
0.5
0.0
-160
-80
0
80
Voltage (mV)
Kv7.1/G219C*/F351A
+ E1
0.4 %ΔF/F
2 s
Kv7.1/G219C*/F351A
+ E1
Relative F/G
1.0
0.5
0.0
-160
-80
0
80
Voltage (mV)

Figure 4

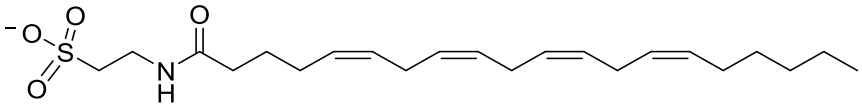

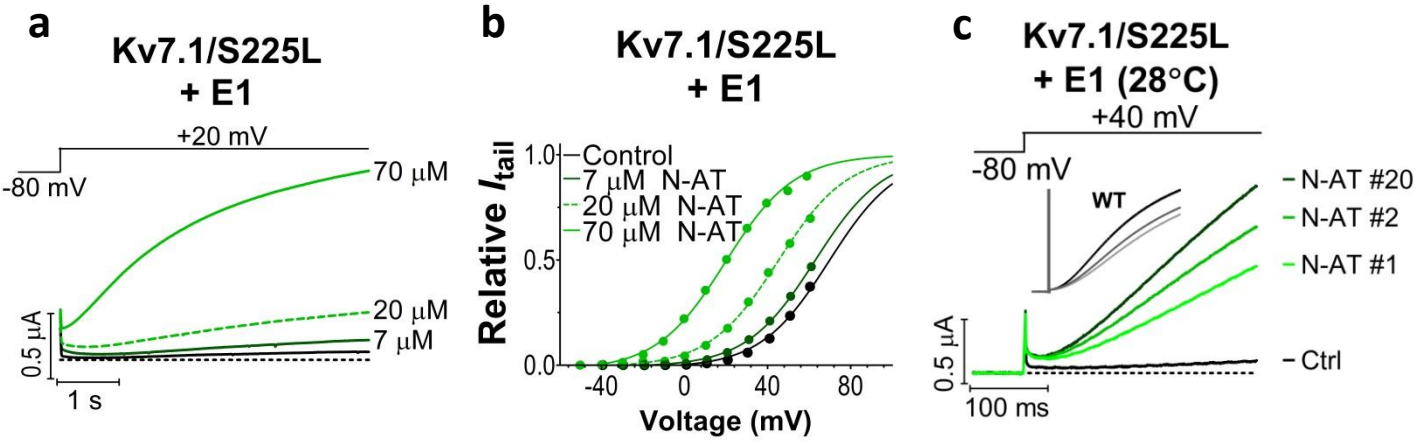
a
Kv7.1/S225L
+ E1
+20 mV
-80 mV
70 μM
20 μM
7 μM
0.5 μA
1 s
b
Kv7.1/S225L
+ E1
Relative I_{tail}
1.0
0.5
0.0
Control
7 μM N-AT
20 μM N-AT
70 μM N-AT
-40
0
40
80
Voltage (mV)
c
Kv7.1/S225L
+ E1 (28°C)
+40 mV
-80 mV
WT
N-AT #20
N-AT #2
N-AT #1
Ctrl
0.5 μA
100 ms

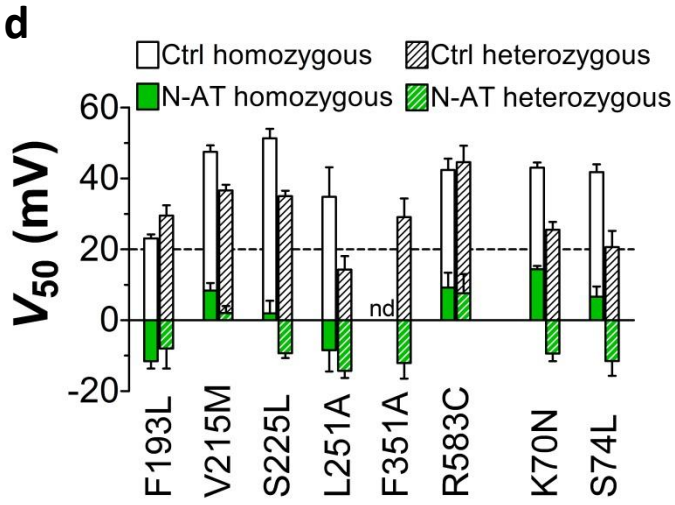
d
Ctrl homozygous
Ctrl heterozygous
N-AT homozygous
N-AT heterozygous
V_{50} (mV)
60
40
20
0
-20
nd
F193L
V215M
S225L
L251A
F351A
R583C
K70N
S74L

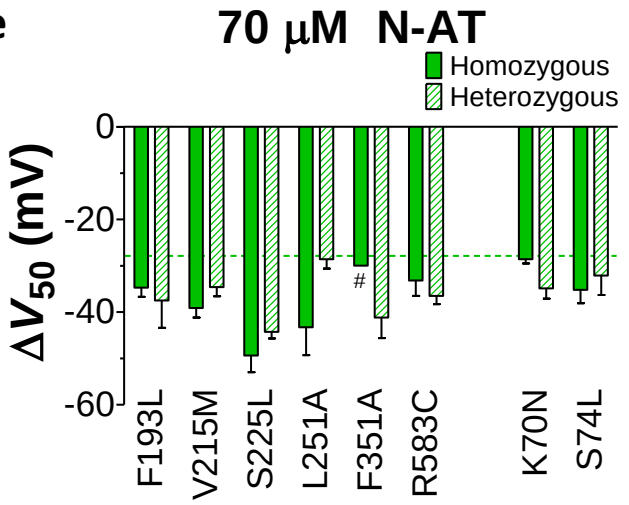
e
70 μM N-AT
Homozygous
Heterozygous
ΔV_{50} (mV)
0
-20
-40
-60
#
F193L
V215M
S225L
L251A
F351A
R583C
K70N
S74L

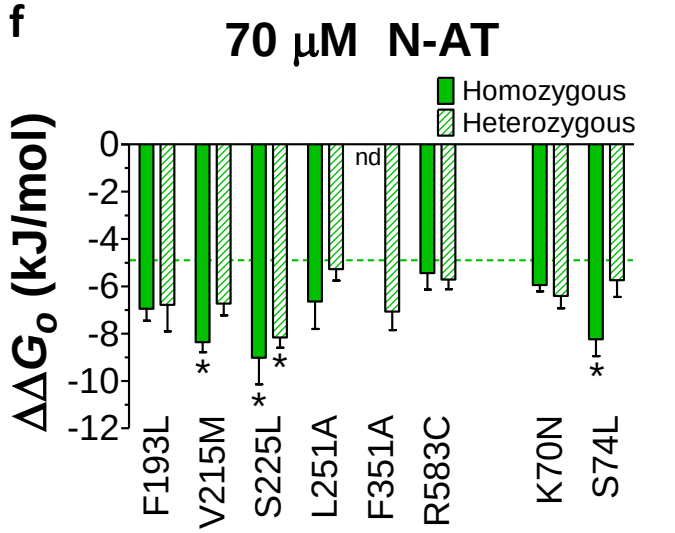
f
70 μM N-AT
Homozygous
Heterozygous
$\Delta\Delta G_o$ (kJ/mol)
0
-2
-4
-6
-8
-10
-12
nd
*
F193L
V215M
S225L
L251A
F351A
R583C
K70N
S74L

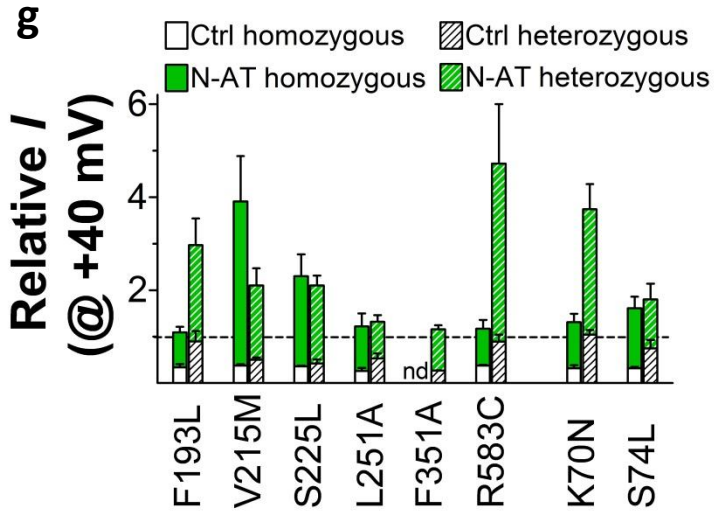
g
Ctrl homozygous
Ctrl heterozygous
N-AT homozygous
N-AT heterozygous
Relative I
(@ +40 mV)
6
4
2
nd
F193L
V215M
S225L
L251A
F351A
R583C
K70N
S74L

Figure 5

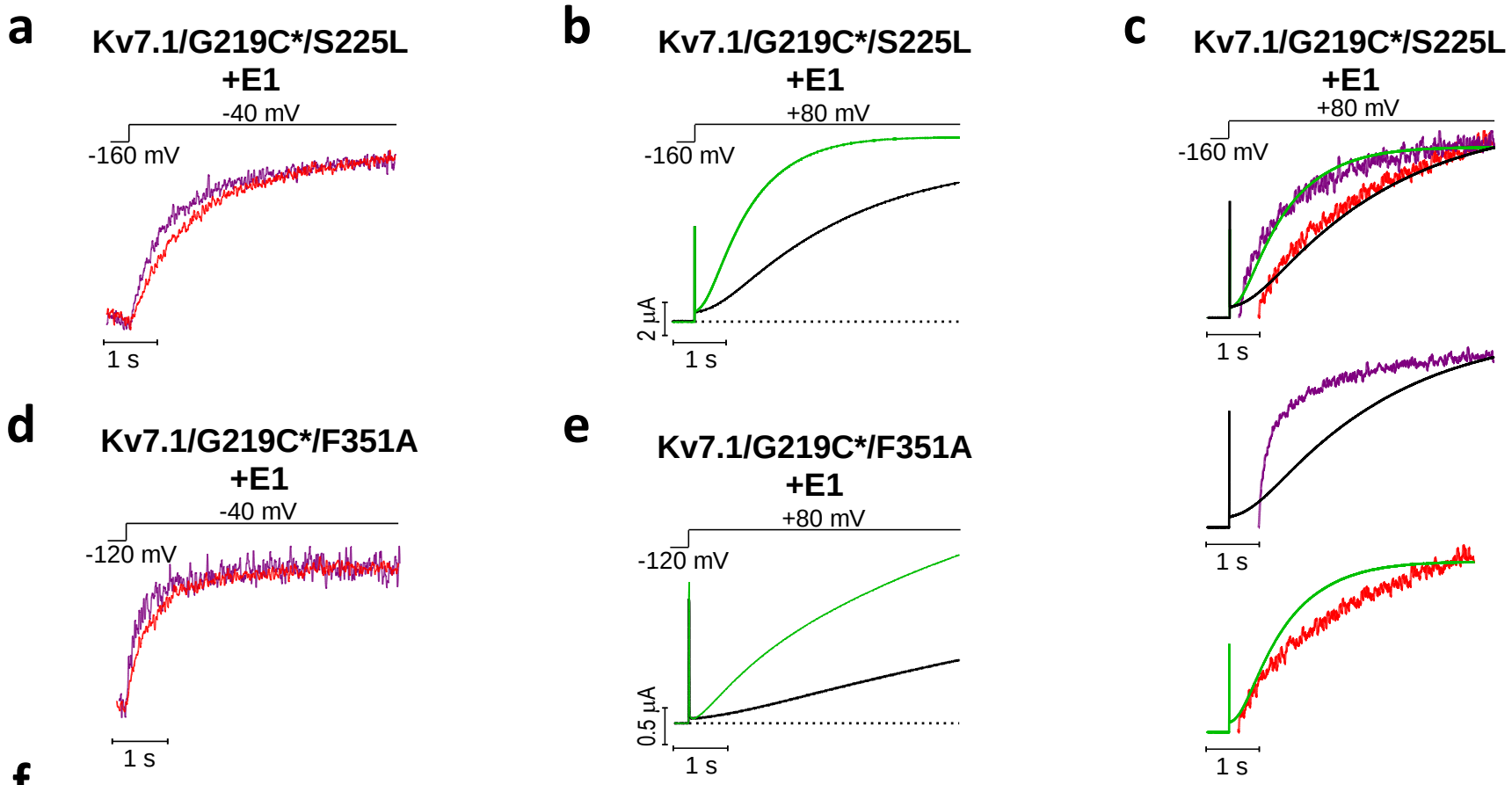

f

	τF_{fast} @ -40 mV (ms)			τF_{fast} @ +80 mV (ms)			τF_{slow} @ +80 mV (s)			τI @ +80 mV (s)		
	Ctrl	N-AT	$\tau_{N\text{-}AT}/\tau_{Ctrl}$	Ctrl	N-AT	$\tau_{N\text{-}AT}/\tau_{Ctrl}$	Ctrl	N-AT	$\tau_{N\text{-}AT}/\tau_{Ctrl}$	Ctrl	N-AT	$\tau_{N\text{-}AT}/\tau_{Ctrl}$
S225L+E1	771±52	481±49	0.64±0.11*	222±14	176±6	0.81±0.06*	2.7±0.2	2.2±0.2	0.81±0.05*	3.2±0.6	0.8±0.2	0.25±0.08**
F351A+E1	560±81	361±59	0.79±0.03*	nd	nd	nd	nd	nd	nd	13.7±3.4	5.6±2.2	0.49±0.15*

Figure 1 – figure supplement 1

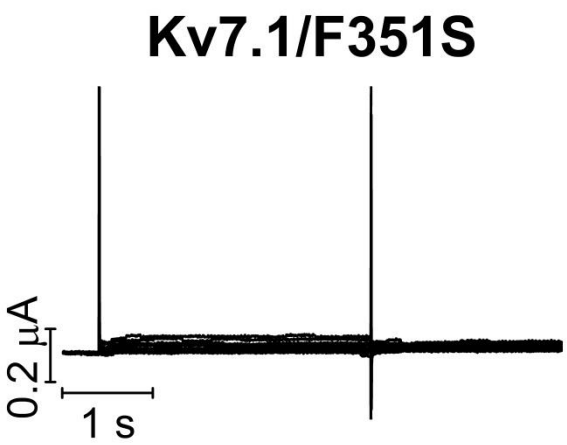

Figure 1 – figure supplement 2

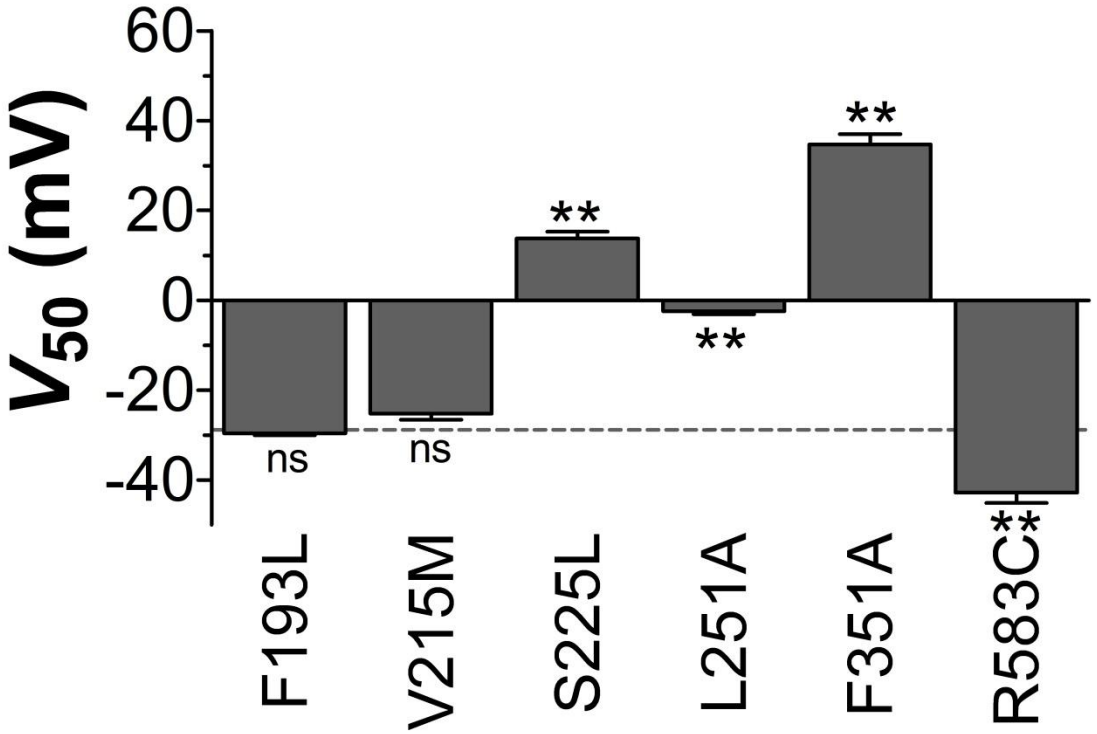

Figure 1 – figure supplement 3

a

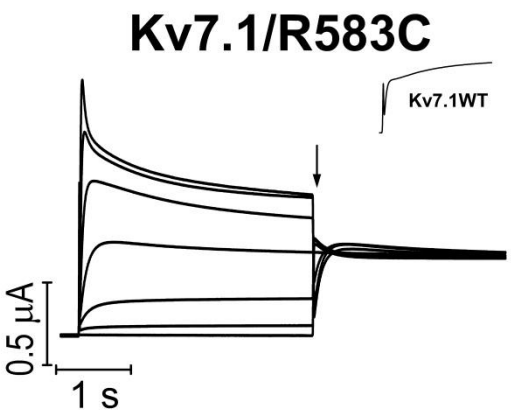

b

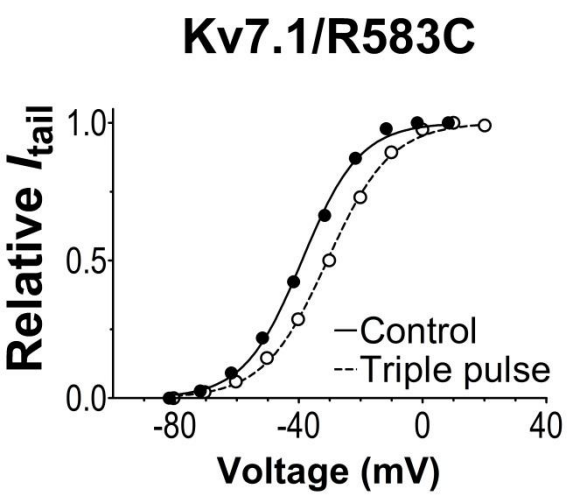

Figure 1 – figure supplement 4

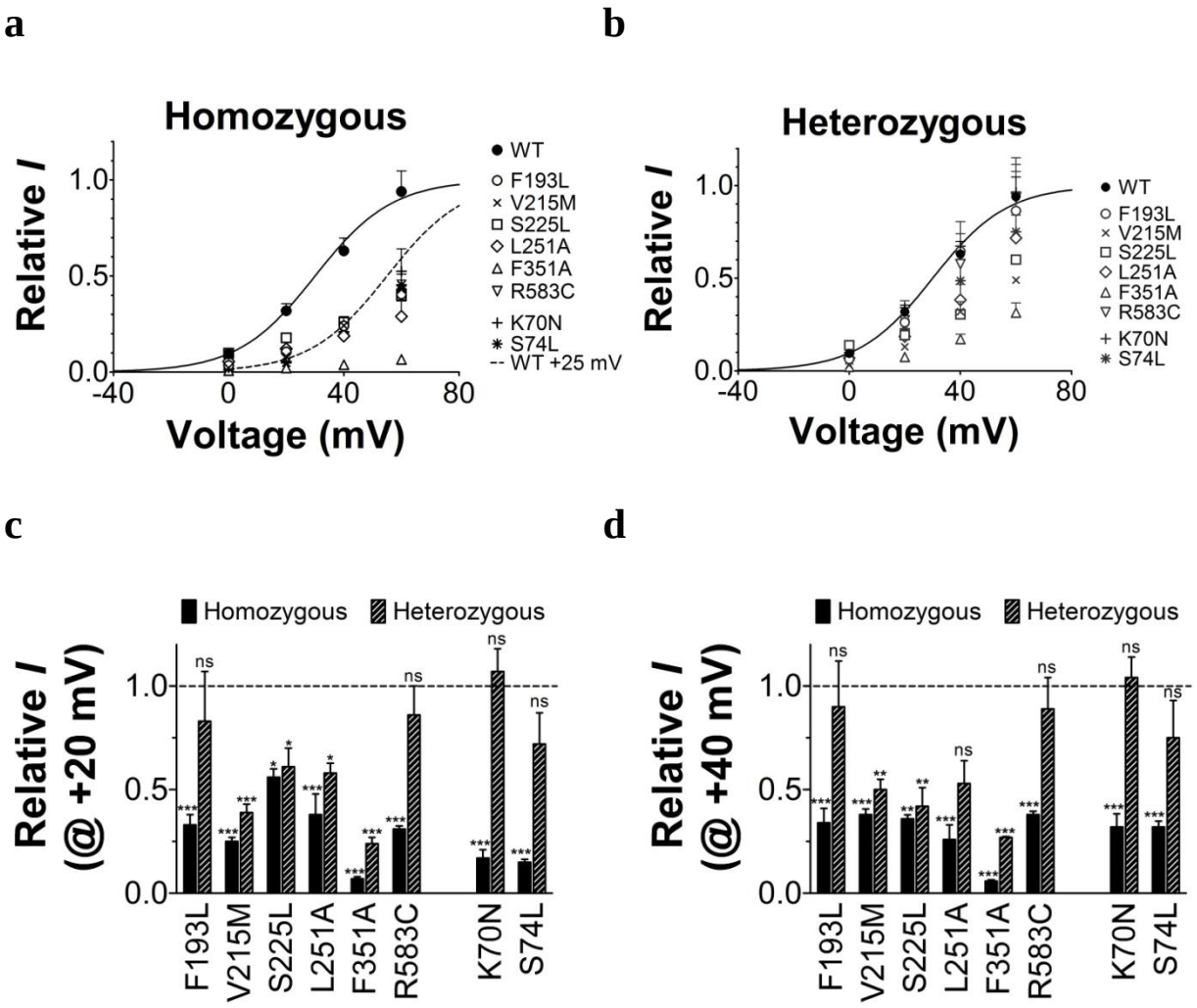

Figure 3 - figure supplement 1

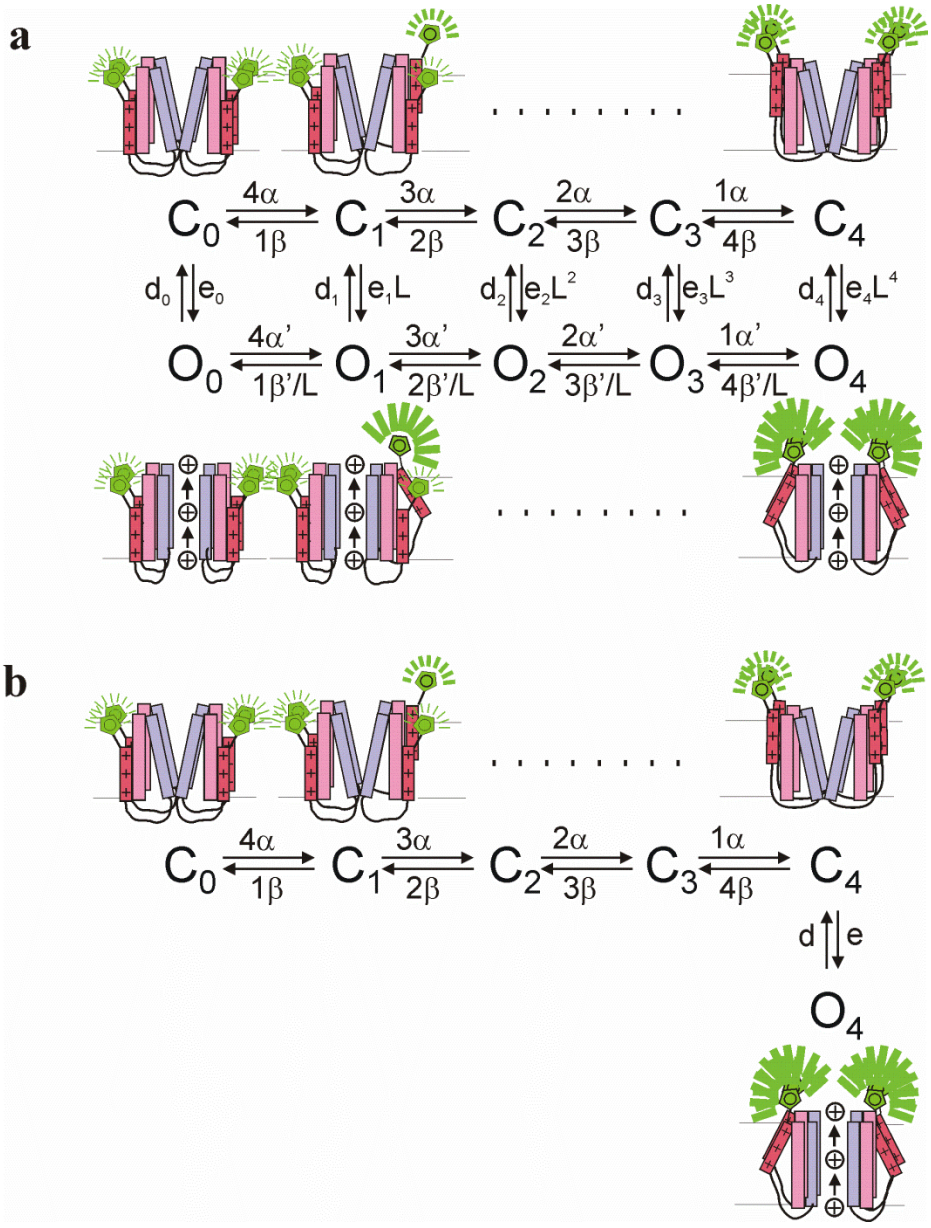

Figure 3 - figure supplement 2

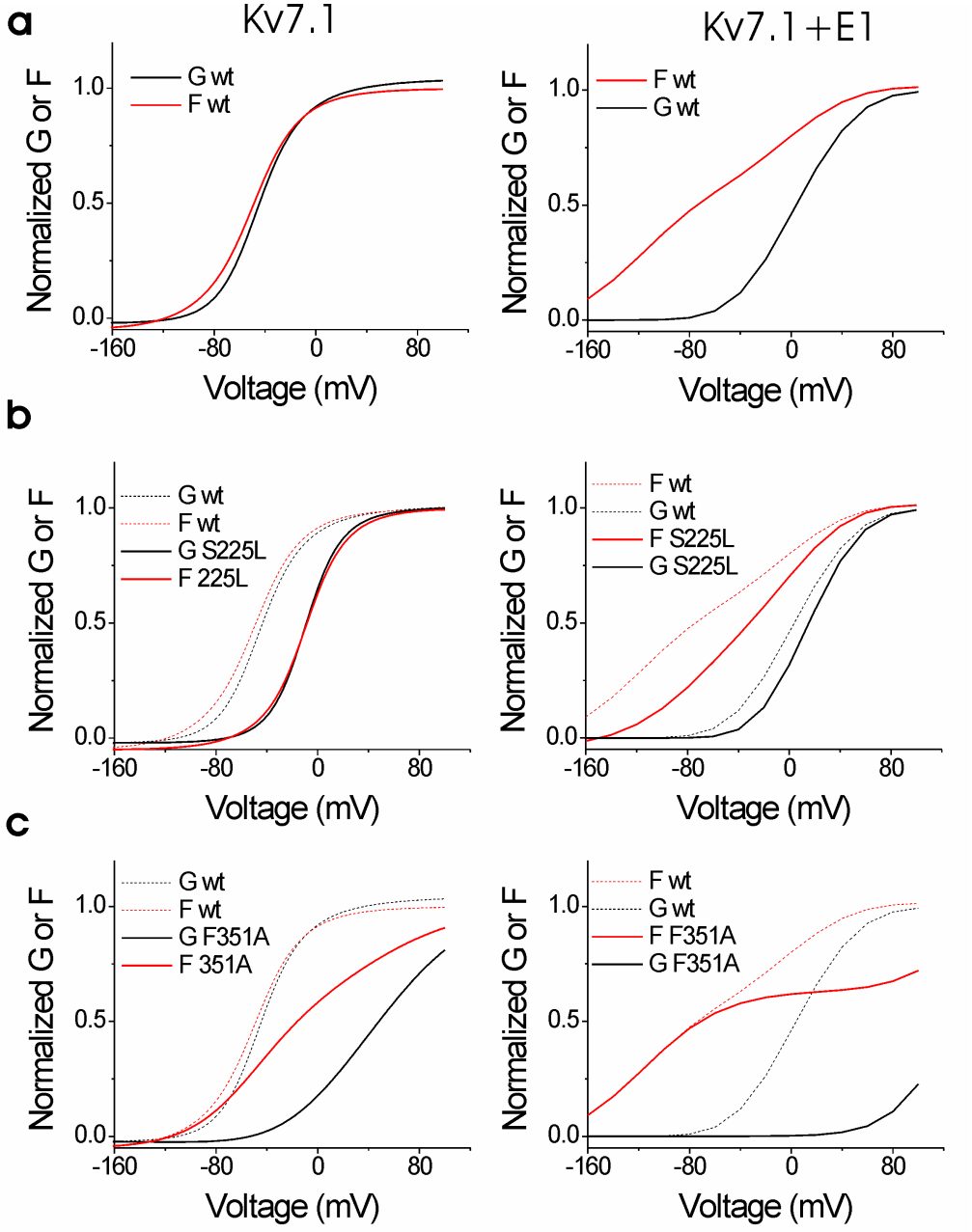

Figure 3 – figure supplement 3

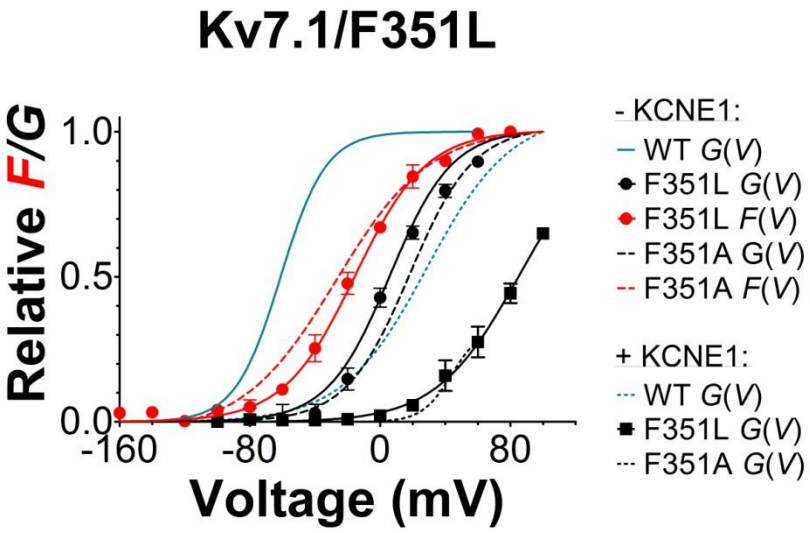

Figure 4 – figure supplement 1

a

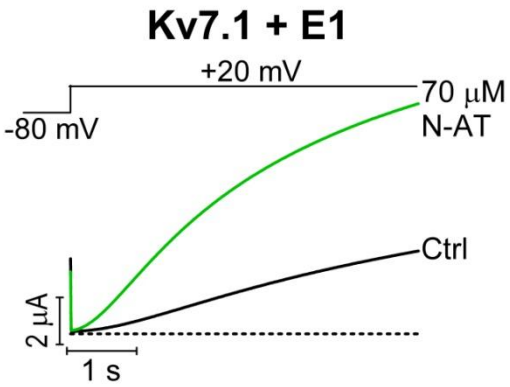

b

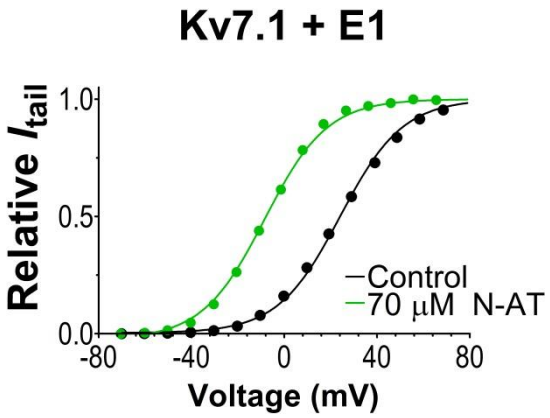

Figure 4 – figure supplement 2

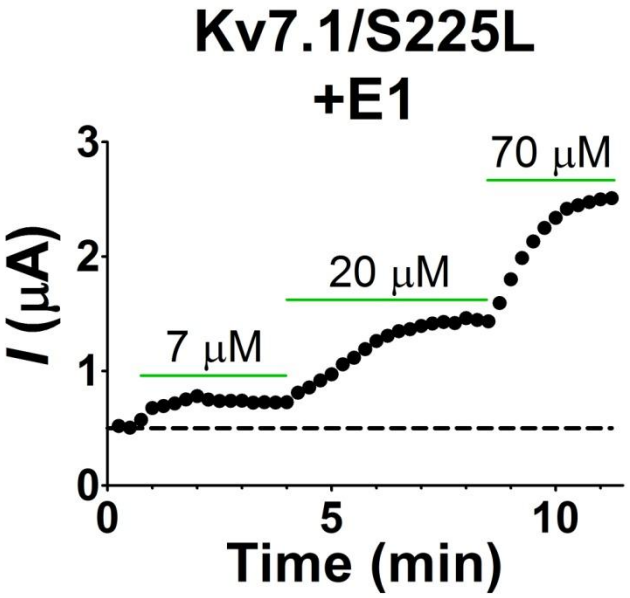

Figure 4 – figure supplement 3

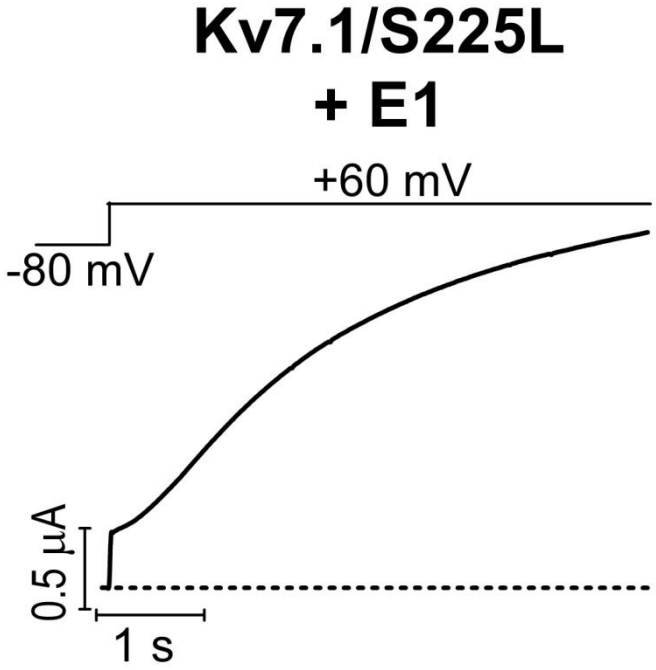

Figure 4 – figure supplement 4

a

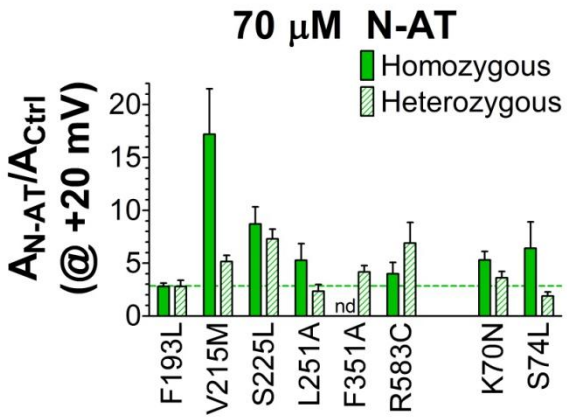

b

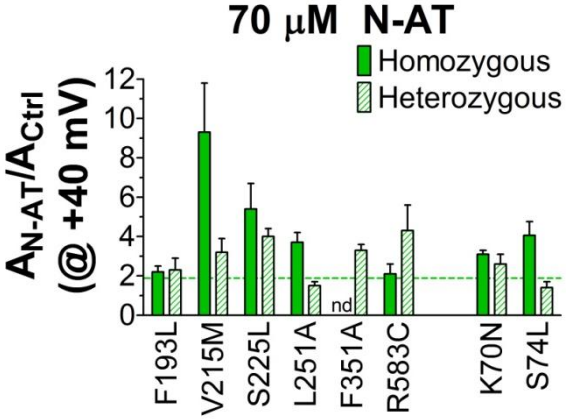

c

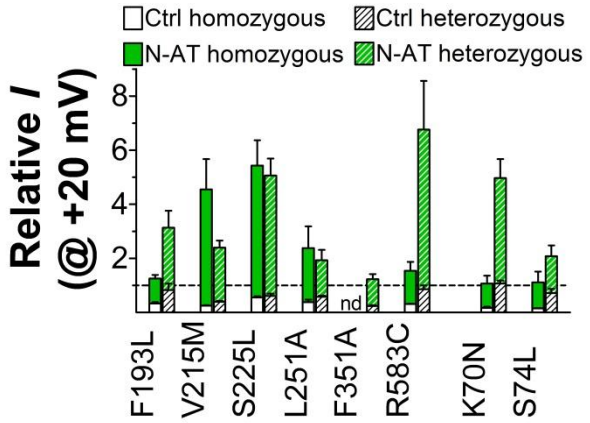

Figure 5 – figure supplement 1

a

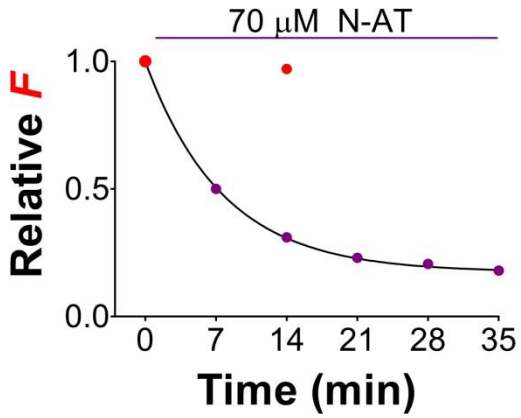

b

	$F_{Alexa488}$ (A.U.)
Control	1.43 ± 0.04
0.25 M N-AT	1.60 ± 0.07
0.5 M N-AT	1.78 ± 0.06

c